MONTE CARLO SIMULATION TO CHARACTERIZE RUNOFF UNCERTAINTY IN A CHANGING CLIMATE

By

GREGORY S. KARLOVITS

A thesis submitted in partial fulfillment of
the requirements for the degree of

MASTER OF SCIENCE IN CIVIL ENGINEERING

WASHINGTON STATE UNIVERSITY
Department of Civil and Environmental Engineering

DECEMBER 2010

To the Faculty of Washington State University:

The members of the Committee appointed to examine the thesis of GREGORY S. KARLOVITS find it satisfactory and recommend that it be accepted.

_____
Jennifer C. Adam, Ph.D., Chair

_____
Michael E. Barber, Ph.D.

_____
Veronica W. Griffis, Ph.D.

_____
Liv M. Haselbach, Ph.D.

Acknowledgements

No part of this thesis would have been possible without the guidance and inspiration of my advisor, Dr. Jennifer Adam. Her knowledge, availability and especially patience, were critical to the completion of my research. I consider myself privileged to have had the chance to work with her. I am also thankful for the valuable input from Dr. Michael Barber and Dr. Liv Haselbach in their effort to bring this thesis to completion. I also wish to thank Transportation Northwest (TransNOW) for funding this project.

I would not have arrived where I am today without the excellent teaching and mentorship I was lucky to receive as an undergraduate at Michigan Tech. Dr. Brian Barkdoll and Dr. Veronica Griffis fostered my interest in hydrology, and Dr. Jake Hiller motivated me to do research.

I am indebted to my good friend Justin Slepak for his assistance and coaching in re-learning computer programming. His help was vital to the completion of my research.

I found our research group to be an excellent source of knowledge and support, so I wish to thank Erika, Josh, Barik, Kirti, Julian and Kiran for the time they shared with me.

Finally, I wish to thank my fiancée Kayleigh for her love and encouragement through the trials and triumphs in completing this thesis. To her I dedicate this work.

MONTE CARLO SIMULATION TO CHARACTERIZE RUNOFF

UNCERTAINTY IN A CHANGING CLIMATE

Abstract

By Gregory S. Karlovits, M.S.
Washington State University
December 2010

Chair: Jennifer C. Adam

Climate change has the potential to intensify precipitation, affecting design storms that are based on historical, stationary data. This decreases the ability to accurately predict the magnitude of runoff due to extreme precipitation events, so a method for assessing the range of possibilities becomes necessary. This paper presents a framework for predicting runoff due to climate change and understanding uncertainty in the prediction.

Historical and future precipitation were modeled with the Generalized Extreme Value distribution fit to the annual maximum 24-hour precipitation event for gridded data at 1/2 degree resolution over the Pacific Northwest (PNW) using the method of L-moments. The rainfall intensities for the 2, 25, 50 and 100-year storms were determined for 1915-2006 and for a number of future climate scenarios for the 2040s, projected by two emissions scenarios and ten global climate models (GCMs).

To determine the range in runoff depths projected due to climate change, Monte Carlo simulation was coupled with the Variable Infiltration Capacity (VIC) hydrology model. For the Monte Carlo simulation, each GCM was weighted by its ability to re-produce 20th century precipitation and temperature over the PNW. Snowpack and soil moisture conditions were simulated for each future climate scenario and fit to a normal distribution. For each return interval, 5000 randomly-selected runoff scenarios varying emissions scenario, GCM, soil moisture and snowpack were simulated with VIC.

The results of the Monte Carlo simulation show increases in runoff for the future with large uncertainty in the forecast of runoff depths. The largest source of uncertainty is from selecting emissions scenarios, which affects all other parts of the projection. The range of runoff was most sensitive to GCM selection and antecedent soil moisture. Scenarios that are warmer and wetter produced the highest runoff forecasts. The most at-risk locations in the PNW, the Puget Sound region and the Olympic Peninsula, were also subject to the largest uncertainty in projecting future runoff depths. We conclude that a probabilistic approach is favorable for assessing the large amount of uncertainty and risk involved in forecasting hydrologic fluxes and states in a changing climate.

Table of Contents

List of Figures

List of Tables

1. Introduction

Recently a great deal of concern has been expressed regarding the potential impacts of climate change. International bodies such as the Intergovernmental Panel on Climate Change (IPCC) or local bodies like the University of Washington Climate Impacts Group (CIG) have attempted to assess the impacts of climate change at various levels. A recent volume of Climatic Change was dedicated to climate change impacts in Washington State (Climatic Change, Vol. 102, No. 1-2, September 2010). Changes in temperature over the next 100 years are projected to occur with high levels of certainty in the Pacific Northwest; these temperature changes are expected to be on average +1.8°C by the 2040s and +3.0°C by the 2080s, compared to the 1970-1999 average (Mote and Salathé 2010). Temperature changes can have a profound effect on the amount, type and timing of precipitation; annual average precipitation volumes can increase or decrease, the ratio of rainfall to snowfall can increase, and the seasonality of precipitation can shift toward wetter winters and dryer summers (Elsner et al. 2010). Hydrology in particular is affected by a changing climate, as the primary driver of the hydrologic cycle is precipitation. This means that current assumptions about water-related engineering designs based on historical climate data may not be adequate in the future (Rosenberg et al. 2010).

Global climate model (GCM) projections for precipitation vary widely spatially and by model. In the Pacific Northwest, there are variations in both sign and magnitude of the projected annual change in precipitation (Hamlet and Lettenmaier 1999, Mote and Salathé 2010). The most consistently forecasted change for precipitation is a decrease in summer volumes when warming is projected to be largest, with a reduction of as much as 20-40% projected by a large

majority (>68%) of models (Mote and Salathé 2010). For winter volumes, the majority of GCMs (>50%) project an increase, with values as high as 42% (Mote and Salathé 2010). However, on average for all models there is a slight increase in annual precipitation, with an average projected change of +1% to +2% (Mote and Salathé 2010).

Frei et al. (1998) hypothesized that future climate scenarios will result in intensified rain events, such that the return intervals for strong storms will decrease; that is, strong storms will occur more frequently. In other words, the intensity of traditional design storms such as the 2-year, 25-year, 50-year and 100-year 24-hour storms will increase in intensity. Rosenberg et al. (2010) and Salathé et al. (2010) agree with this hypothesis on a regional basis for the Pacific Northwest.

As there is uncertainty in the eventual effects of climate change on precipitation, understanding the range of projected scenarios is important. Intensification of extreme events would result in the need for modification of current design practices as well as the enhancement of existing infrastructure meant for handling runoff (Rosenberg et al. 2010).

Standard design practices for hydraulic structures are based on the prediction of events and the allowable risk associated with them (Chow et al. 1988). Depending on the sensitivity of the structure and the desired performance in response to some event, a structure is designed based on the probability that an event, such as a rainfall or runoff volume, will not be exceeded. This is achieved by assessing the probability that an event will or will not occur by the use of statistics. The events of the past are used to determine the potential for one to occur in the

future. This assumes independence of the variables, the same underlying distribution for the data, and stationarity of the data (Milly et al. 2008, Chow et al. 1988).

Human disturbances in river basins, such as land use change, have long compromised the assumption of stationarity within probability density functions governing uncertainties, affecting the predictive ability of planners and engineers (Milly et al. 2008). A loss of stationarity is caused by a change in variance or mean in time for the system being statistically modeled (Chow et al. 1988). As discussed, substantial anthropogenic change of Earth's atmosphere, and therefore climate, is altering many hydrologic parameters, including the mean and extremes of precipitation causing a loss of stationarity (Milly et al. 2008). Because any ability to predict future risks associated with precipitation events rests on the ability to utilize historic data with the assumption that it still applies, it is clear that climate change is affecting the ability to assume that this is still valid.

Hydraulic structures that are designed to withstand more extreme events, in other words structures that failure should not be risked, e.g. major dams, may be designed to control a precipitation or streamflow event with a return interval of 50-100 or more years (Chow et al. 1988). When there is a risk of loss of life or significant economic or social damage, the use of longer return intervals is often justified. The difficulty in estimating the magnitude of these events often lies in the inadequate period for data of record and poor choices in methodology for estimating design events (Wohl 2000, Linsley 1986). Thus, the intensity of the 100-year storm or flood may be estimated based on merely 50 years of rainfall or streamflow data. While this is difficult to consider statistically defensible, it is often the only means available to

estimate the risk. If one takes into account that these 50 years are affected by a loss of stationarity, the effective length of the precipitation record decreases (Tasker 1983). This results in higher error in the estimation probability density functions and therefore a lower confidence in the ability to design a structure that will not fail within its lifetime of service.

The use of GCMs to project the future climate based on emissions scenarios is one way to improve the ability to predict these future events. By running these GCMs, probability density functions can be constructed to represent the probability of future events occurring. While the result of running these GCMs is sensitive to a number of factors, including time period modeled, choice of GCM, downscaling method, emissions scenario and more, these results are better than assuming stationarity of non-stationary data. With an appropriate choice of GCM, downscaling technique and other hydrologic model parameters, a range of uncertainty can be assessed for future projections for precipitation events.

This research aims to investigate the effects of climate change, in terms of the change in the intensity of commonly-used design storms, on runoff in the Pacific Northwest. The Variable Infiltration Capacity (VIC) large-scale hydrology model (Gao et al. 2010, Liang et al. 1994) is applied to the Pacific Northwest to model the runoff due to storms of an intensity corresponding to 2, 25, 50 and 100-year average return intervals (ARI). The intensity of these storms will be estimated for the historical 1915-2006 climate and compared to downscaled projections by a suite of GCMs forced with two different greenhouse gas emissions scenarios.

This study seeks to answer two questions regarding climate change and runoff:

1. How will climate change in the Pacific Northwest affect the amount of runoff generated by design storms of common return intervals, comparing historical climate to GCM-simulated future climate?

2. How much uncertainty in projecting runoff in the future is caused by selection of greenhouse gas emissions scenarios, GCMs, and hydrologic modeling of snowpack and soil moisture for future climate scenarios?

2. Data, Models and Methods

To identify the major sources of uncertainty in projecting the effects of climate change on runoff generation from specific design storms, we isolated the contributions of uncertainty to individual inputs to a hydrologic model, which is a tool used to identify tangible effects of climate change. In this case we examine changes in runoff. By understanding the uncertainty in the model inputs, we are able to improve forecasts for runoff in the future by giving more weight to "better" or more likely predictors of runoff in the future. The methods in this study allow us to present a range of results that arise from a large number of combinations of probable outcomes.

2.1 Study Area

In this study, the Pacific Northwest was defined as the Columbia River basin, as well as areas west of the basin that drain into the Pacific Ocean, including coastal Oregon, the Puget Sound region of Washington, and the low-lying area around Vancouver, BC. See figure 1 for an

elevation map of the region, derived from 1/16 degree soil parameters (Elsner et al. 2010). The Pacific Northwest has several types of dominant climate. The region contains temperate coastal rainforests, glaciated mountain rangers and arid scrublands (Salathé et al. 2010). The coastal region, bordered by the Pacific Ocean on the west and the Cascade Mountains on the east, experiences wet, mild winters and dry, warm summers (Waring and Franklin 1979). The state of Washington itself, which comprises a large portion of the study area, is characterized by complex terrain and coastlines, which contributes to weather systems with varying spatial and temporal characteristics (Salathé et al. 2010). Also due to the orographic effects of the Olympic and Cascade Mountains and the Canadian range of the Rocky Mountains, the windward slopes of these features can receive extensive annual totals of precipitation (Elsner et al. 2010). Figure 2 shows average annual precipitation for the Pacific Northwest for the years 1915-2006 as derived from 1/16 degree gridded daily meteorological data (Elsner et al. 2010). The drying effect of the mountain ranges creates a semiarid climate in the interior region of the states of Oregon and Washington which receives about a quarter of the total rainfall that occurs on the western side of the mountains (Elsner et al. 2010). This area is less densely populated than the areas west of the Cascade Range and is commonly used for dryland farming, as in the Palouse region of eastern Washington, or heavily irrigated farming practices, such as Yakima County in the eastern Cascade rain shadow.

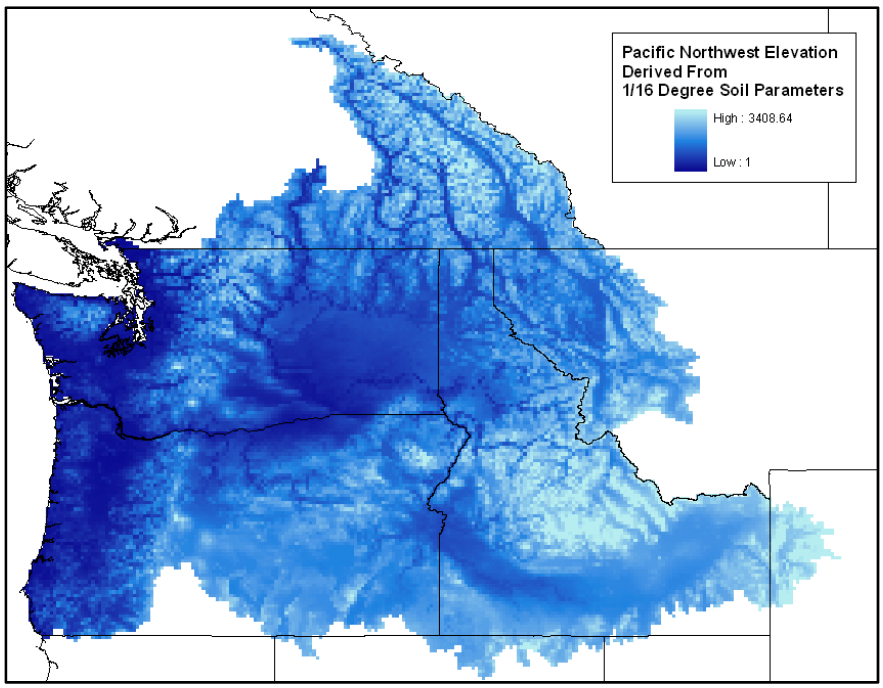

Figure 1: Elevations in the Pacific Northwest as derived from 1/16 degree soil parameters from Elsner et al. (2010)

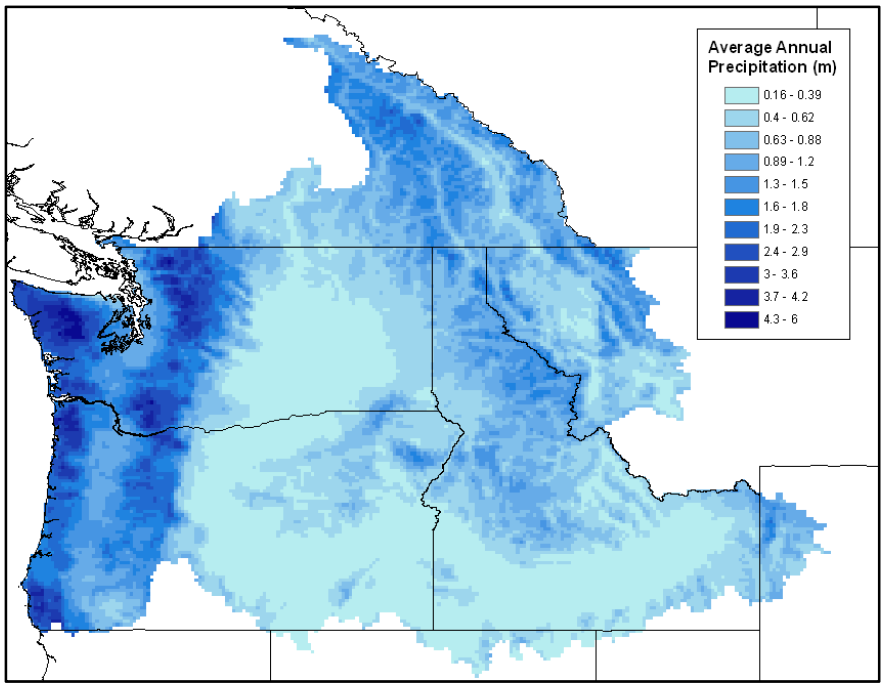

Figure 2: Pacific Northwest annual average precipitation for 1915-2006 as derived from 1/16 degree daily meteorological data (Elsner et al. 2010)

Runoff concerns are different between these two distinct regions due to their differing precipitation regimes. For example in western Washington and other coastal areas, storms are typically of long duration but low intensity, but in eastern Washington and Oregon storms are of shorter duration but higher relative intensity. The State of Washington issues two separate stormwater management guides through the state Department of Ecology, dividing western and eastern Washington in terms of their stormwater requirements (Labib and O'Brien 2005 and Washington Department of Ecology 2004, respectively). Due to the precipitation regimes, hydrologic analysis for stormwater in western Washington requires continuous simulation for land-use changes at a 1-hour timestep in HSPF (Hydrologic Simulation Program – Fortran) (Labib and O'Brien 2005, Bicknell et al. 1997). The eastern Washington manual requires single-event hydrograph methods, such as the SCS hydrograph or the Santa Barbara Urban Hydrograph (SBUH) (Washington Department of Ecology 2004). Specified storm distributions for short (3-hour) or long (24 or more hours) storms are provided in the manual for application to certain types of stormwater best management practices (BMPs).

2.2 Design Storms

Engineers often characterize precipitation events used for designing water control structures by their average return interval (ARI) (Chow et al. 1988). The ARI is given as an average, or expectation, of the period between occurrences of an event. Its definition arises from equation (1):

$$T = \frac{1}{1-p} \tag{1}$$

where T is the ARI in years and p is the probability of the event of interest *not* being exceeded in a given year. Thus, a storm intensity that has a 1% chance of being exceeded in a year has a probability of 0.99 of not occurring in a year. This is called the *100-year event* on account of the expectation of its exceedance occurring once in 100 years. However, the occurrence of these events is probabilistic and is not fixed according to the return interval and can occur at any time (Bedient et al. 2008). The probability of at least one event in n years exceeding the T-year event is given in equation (2) and is also called the risk function (Bedient et al. 2008):

$$r = 1 - \left(1 - \frac{1}{T}\right)^n \tag{2}$$

Additionally, the probability of exactly x events exceeding the T-year event in an n-year period is given in equation (3):

$$p_{x,n} = \binom{n}{x}\left(\frac{1}{T}\right)^x\left(1 - \frac{1}{T}\right)^{(n-x)} \tag{3a}$$

where $$\binom{n}{x} = \frac{n!}{x!(n-x)!} \tag{3b}$$

These probabilistic tools help planners and engineers quantify the risk that a water control structure has based on the acceptable probability of the failure of that structure during its design lifetime. However, the challenge in assessing these risks comes from estimating the probability of these events.

Typically two kinds of events are described using return intervals in hydrology: rainfall events ("storms") and streamflow events ("floods"). What is important to note is that the events are generally causally independent; the 100-year storm does not necessarily cause the 100-year flood (Rahman et al. 2002). The occurrence of the 100-year flood is dependent on more than just the input of precipitation and can include the presence of more influences on the runoff system such as antecedent soil moisture (Wei et al. 2007), antecedent snowpack volumes (Marks et al. 2001) and prior streamflow conditions. In this study, to quantify the actual effect of extreme rainfall events such as the 50- or 100-year storm, the storm event is used as input to a model to evaluate the effect of such an event in terms of the runoff it generates.

2.3 The VIC Hydrology Model

Runoff is a component of the water balance that is often of concern to those dealing with handling water and preventing flooding, so there are a multitude of models and methods for determining the amount of runoff generated by a storm event or with a series of meteorological data. They vary widely by parameterization and method for solving the water and/or energy balances that govern the hydrologic cycle.

The model used in this study is the Variable Infiltration Capacity (VIC) macroscale hydrology model, developed at the University of Washington (Gao et al. 2010, Liang et al. 1994). It is a fully-distributed, continuous hydrology model comprised of large grid cells with sub-grid heterogeneity of land cover and elevation handled with statistical distributions. Although it is capable of being run at a spatial resolution as fine as 1/16 degree, the model was run at 1/2

degree in the interest of computation time.VIC produces a gridded result for fluxes and states within each grid cell as defined by the resolution, and as such, producing a streamflow hydrograph is handled by a separate routing model (Lohmann et al. 1996). In this study only gridded runoff depths will be considered for the comparative analysis. Because the fluxes of each cell are computed separately, and no flow occurs between the cell boundaries, conditions for each grid cell can be explored separately without competing interaction from neighboring cells. It is assumed that the grid cells are large enough within the model that these interactions are negligible. VIC is capable of simulating frozen soils, but this feature was not used as most regions in the study were simulated for non-winter months. The regions that were simulated for winter months, e.g. the western side of the Cascades, do not commonly encounter frozen soils. Not using frozen soils would cause a systematic low bias in regions where the effect of frozen soil on runoff is significant. In general, frozen water in soil pores reduces rates of infiltration thereby producing more runoff during an event than in unfrozen conditions (Cherkauer and Lettenmaier 1999).

VIC input data include soil parameters, land cover parameters, topography, and meteorological forcing data. Parameters for soil and land cover over the contiguous United States were those developed and described in Maurer et al. (2002) originally at 1/8 degree resolution. Elsner et al. (2010) redefined these parameters over the PNW at 1/16 degree. The 1/16 degree data were aggregated to 1/2 degree. The soil parameters were originally from a 1 km dataset from Pennsylvania State University (Miller and White 1998) and for locations outside the US from the 5-minute FAO set (FAO 1998). The vegetation parameters were derived from 1 km global data from the University of Maryland (Hansen et al. 2000).

2.4 Synthetic Meteorological Data

Testing changes in climate, as represented by changes in meteorological forcing, particularly the change in the intensity of precipitation, is one of the key objectives of this study. To compare consistent measures of precipitation intensity over the entire domain, design storms with commonly-applied return intervals were selected for comparison analysis between the historical and GCM-projected future climate. In order to test isolated, hypothetical storm events for their impact on runoff, VIC was run in "event" mode, and thus, meteorological data for testing those events were synthesized.

The goal of creating "synthetic" meteorological data was to create a climate dataset that represents realistic temperature and wind conditions for the design storms being tested for each grid cell in the domain. This consisted of determining when the annual maximum events tended to occur, and what the weather conditions were like, on average, for that time period.

Synthetic meteorological data for the storm events of interest were created in a several-step process. First the 1/16-degree data were aggregated to 1/2-degree resolution. All 1/16-degree data for historical climate and downscaled future climate are from Elsner et al. (2010). At 1/16-degree resolution it was assumed that the entirety of each cell contributed to the study domain. The aggregation results were checked by comparing the mean and variance of each parameter over the basin for each step of aggregation. As expected, the mean of each parameter remained nearly constant while the variance decreased slightly, due to the smoothing effects of averaging. The averaging of precipitation data leads to an underestimation bias for extreme

events, because the most intense events are averaged with events of a smaller magnitude in the neighboring contributing cells when aggregated.

2.4.1 Rainfall Statistics

To assess the frequency-intensity relationship in annual precipitation patterns, historical and projected future precipitation characteristics were modeled statistically. A distribution was fit to the data in order to estimate the intensity of the storm associated with an ARI of interest. In order to model the data, the annual maximum 24-hour storm intensity was selected to fit the data. Annual maxima of a time series, producing an annual maximum series, tend to satisfy the important assumption for modeling data statistically that the data are independent and identically distributed, 'i.i.d.' (Chow et al. 1988). By choosing the annual maximum series, a distribution can be fit to the data and quantiles (the magnitude of an event associated with some probability) can be estimated. Because the annual maximum data are located in the extreme upper tail of the probability distribution of all of the data they are drawn from, they have a different probability distribution than the parent population (Chow et al. 1988).

However, because the time-step of the meteorological dataset was 24 hours, the analysis utilized the largest calendar day precipitation total for each year instead of the largest 24-hour precipitation event. Because storm events could potentially occur overnight, with rainfall divided over two days and producing a 24-hour precipitation total that is not represented by calendar days, a systematic low bias for the 24-hour annual maximum event was introduced. Additionally, in order to assess the impacts of changing climate on runoff specifically, only

liquid precipitation events were selected. This was done by only testing if a precipitation event was an annual maximum when the daily minimum temperature was greater than 0 °C.

There are many distributions used to model hydrologic variables with varying degrees of simplicity in application and goodness of fit (Chow et al. 1988). Rosenberg et al. (2010) modeled precipitation values using the generalized extreme-value distribution (GEV). Mannshardt-Shamseldin et al. (2010) successfully utilized the GEV distribution for modeling gridded precipitation data with a long record such as the data in this study. The GEV distribution incorporates three distinct distributions, the Gumbel (GEV type I), Fréchet (GEV type II) and Weibull (GEV type III) distributions by means of estimate of the shape parameter of the distribution (Chow et al. 1988). For this study, due to its simplicity and flexibility of application, the GEV was used to model rainfall extremes in the Pacific Northwest.

In order to model data with a distribution, the parameters of the distribution must be estimated. Parameters of a distribution determine the "shape" and behavior of the probability and cumulative density functions. They are the expected value of some function of a random variable (Chow et al. 1988). For example, the parameters of the normal distribution are the mean and standard deviation (Chow et al. 1988). There are a few methods employed to estimate the parameters of a distribution, including the method of moments (MOM), maximum likelihood estimators (MLE), and L-moments (Chow et al. 1988, Mannshardt-Shamseldin et al. 2010). These methods attempt to discern the parameters of the population based on those of the sample.

The methods found in Rosenberg et al. (2010) and Hosking and Wallis (1997) employed use of a distribution fit by use of L-moments. The studies in Zwiers and Kharin (1998) and Kharin and Zwiers (2000) specifically used the GEV distribution fit with L-moments to assess the intensity of extreme climate under global warming scenarios. The use of L-moments is found extensively in hydrology and other geospatial statistics and is popular with hydrologists and meteorologists (Mannshardt-Shamseldin et al. 2010). The method of L-moments is an alternative method to the conventional descriptions of a distribution's shape (Hosking and Wallis 1997). Conventional product-moment coefficient of variation (CV), skew and kurtosis are highly variable and are biased based on the sample size and underlying distribution (Wallis et al. 1974). L-moments can describe properties of a distribution and estimate the CV, skew and kurtosis from samples based on probability weighted moments (PWM) (Hosking and Wallis 1997). L-moments are linear combinations of PWMs and do not involve taking higher powers (such as squaring in the case of variance or cubing in the case of skewness) of observations, and have better sampling properties than conventional sample moments, which can better describe a sample of extremes in different probability distributions (Zwiers and Kharin 1998, Hosking 1992). Statistical distribution parameters can be determined from the L-moments of a sample.

Because the GEV distribution has an explicit form of the inverse of the cumulative distribution function, also known as the quantile function (Gilchrist 2000), the intensity of events with a specific probability of non-exceedance can be computed given the distribution parameters as fit to the precipitation data.

If the ARI for an event is defined in equation (1) where T is the ARI in years, given p, the probability that the event will not be exceeded in a given year, then the quantile function for the GEV distribution is defined in equations (4a) and (4b):

$$x_p = \xi + \frac{\alpha}{\kappa}\left[1 - \left(-ln(p)\right)^{\kappa}\right] \qquad \text{when} \quad \kappa \neq 0 \tag{4a}$$

$$x_p = \xi - \alpha\, ln[-ln(p)] \qquad \text{when} \quad \kappa = 0 \tag{4b}$$

where x_p is the magnitude of the event corresponding to the non-exceedance probability p (the "T-year storm"), and the Greek letters alpha (α), kappa (κ) and xi (ξ) are the parameters of the GEV distribution as determined by the L-moments fit. Alpha (α) is the scale parameter, xi (ξ) is the location parameter, and kappa (κ) is the shape parameter; the shape parameter determines the type of extreme value distribution and the bounds of the function (Zwiers and Kharin 1998). For each grid cell the parameters were estimated using an L-moments fit and the extreme precipitation was modeled specific to each cell. As such, the feasibility of the parameters for each grid cell needed to be checked (Kharin and Zwiers 2000). Estimates for the parameters must satisfy the constraints in equations (5a) and (5b):

$$X_{n:n} \leq \xi + \frac{\alpha}{\kappa} \quad (\kappa > 0) \tag{5a}$$

$$X_{1:n} \geq \xi + \frac{\alpha}{\kappa} \quad (\kappa < 0) \tag{5b}$$

where $X_{n:n}$ is the largest value in a sample of size n and $X_{1:n}$ is the smallest. Non-feasible (constraint-violating) parameter estimates occur less than 1% of the time for values of $\kappa \leq 0.1$

and more often for larger values of κ (Dupuis and Tsao 1998). Unlike the estimate for other parameters, the frequency of occurrence of non-feasible parameter estimates is not improved with a larger sample size (Dupuis and Tsao 1998). All data were checked for compliance with the constraints and found that the parameter estimates were feasible for the entire domain, so no methods to estimate alternative feasible values of κ, such as those in Dupuis and Tsao (1998) or Kharin and Zwiers (2000) needed to be applied.

As the probability of an event was defined in equation (1), the quantile represents a 24-hour precipitation intensity that is expected to not be exceeded with a probability of p in a given year, or will, on average, occur once in T years. For this study the 2-year, 25-year, 50-year and 100-year 24-hour annual maximum precipitation events were considered, corresponding to non-exceedance probabilities of 0.50, 0.96, 0.98 and 0.99, respectively. Return intervals of 25, 50 and 100 years are common for water control structures of moderate risk where probability-based limits are practical for assessing risk (Chow et al. 1988). The 2-year storm is being included in this study as it represents the median annual exceedance event; that is, the event expected to be exceeded in 50% of years.

As both the precipitation data and model simulations were at a 24-hour timestep, no attempt to disaggregate the precipitation events into a sub-daily distribution was made. Loukas and Quick (1996) found that heavy precipitation events in southwestern British Columbia, part of the study domain, were reasonably uniform temporally. Thus the model would consider each precipitation event to be uniform over the 24 hour period of the model run and the outputs for runoff would be the same 24-hour average depth.

A limitation to the large-scale model is the coarse resolution. Because the model is being run at 1/2-degree resolution, the area covered by each grid cell is very large, with grid cells about 56 km on a side at the equator. Spatially distributed parameters such as land cover, soil and elevation are not explicit in their location within the grid cell. This makes it difficult to project the effect of changing runoff on a scale relevant to local stormwater applications, which typically are designed for lower non-exceedance probabilities, as they are considered less risky and require a smaller degree of protection (Chow et al. 1988). Thus the emphasis is placed on storms with a longer ARI.

2.4.2 Average Climate for Annual Maximum Events

After the annual maximum series were fit to a distribution, the dates of each of the peak events for the 92 years of record were put into a histogram with a bin width of 14 days and the peak bin was selected from the series. The seasonality of the rainfall events is apparent in figure 3, which illustrates the season which most frequently had the annual maximum event in each grid cell over the 92 years of record. The results in figure 3 agree with Elsner et al. (2010) in terms of the winter dominance of rainfall west of the Cascades. For each cell, the date of the middle of the peak bin was used for choosing the date for distributing the soil moisture and snow water-equivalent (described in 2.5 and 3.3). The two-week period surrounding that date was used for finding an average climate present around the time of peak annual precipitation.

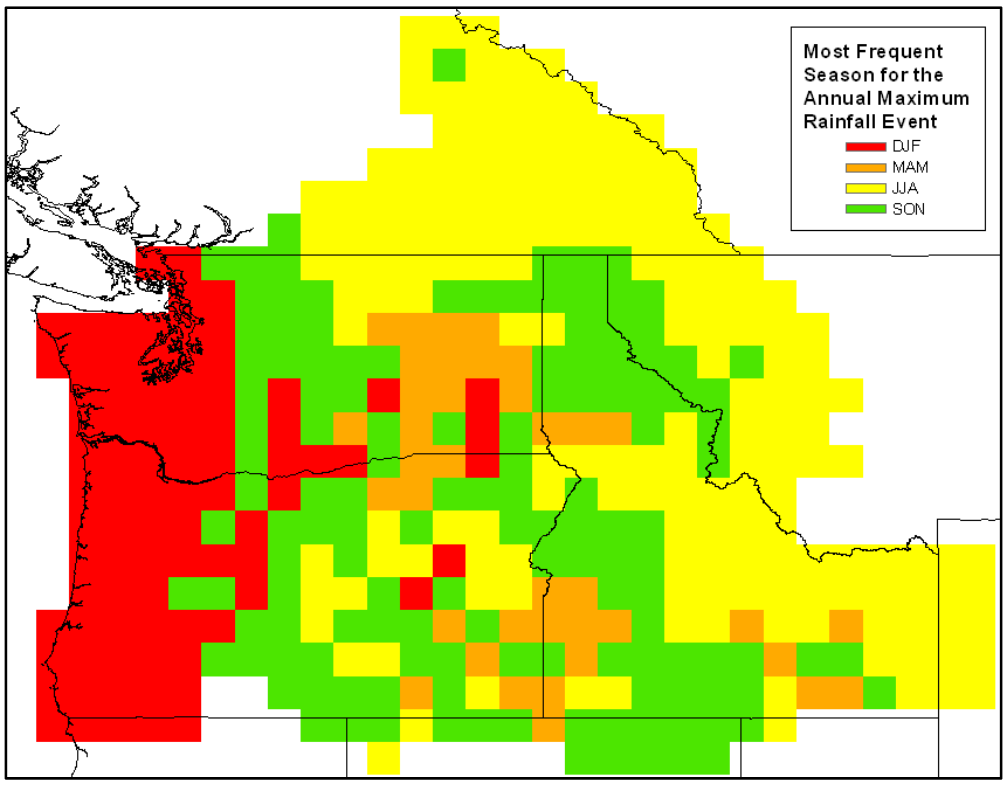

Figure 3: Most frequent season of annual maximum rainfall event for the Pacific Northwest at 1/2 degree, years 1915-2006, aggregated from 1/16 degree meteorological data from Elsner et al. (2010)

For those 14 days in each of the 92 years of the meteorological record the daily maximum temperature and minimum daily temperature were extracted. Because wind speed values were downscaled from the NCEP-NCAR reanalysis, the wind speeds were only considered valid for the years 1949-2006, which is the period for the reanalysis data (Kalnay et al. 1996). The 1288 sampled days for temperature and 812 days for wind speed were averaged and used to create new synthetic meteorological data. By sampling the weather individually by cell, locations within the Pacific Northwest with different storm characteristics could be represented in a way that describes a common scenario for the occurrence of extreme precipitation events. For each GCM and emissions scenario, the weather conditions for the simulated peak date in each grid cell were used in the synthetic meteorological data for the design storms being tested, therefore

the temperature and antecedent soil moisture and snow water-equivalent conditions will respond to a different realization of future climate according to emissions scenario and GCM.

2.5 Monte Carlo Simulation of Runoff Response

Monte Carlo simulation is a technique that uses random or pseudorandom numbers in order to find a solution to a problem (Rubenstein 1981). It achieves an approximate solution of a mathematical or physical problem by simulating random quantities (Sobol 1974). The Monte Carlo method was first described in a summary by Metropolis and Ulam of the Los Alamos National Laboratory in 1949 as a method for solving large systems in particle physics by means of what was called "statistical mechanics." It represented a departure from the study of classical mechanics of individual particles to the statistical study of *sets* of particles, thereby combining statistics with the then-new field of set theory (Metropolis and Ulam 1949). Cashwell and Everett (1959) used the method to illustrate particle physics in which a particle's behavior was described probabilistically for all situations it potentially encountered in its history. The name "Monte Carlo" comes from the city of the same name in Monaco, famous for gambling (Sobol 1974). The Monte Carlo algorithm, in general, consists of a process for generating a random event of some kind, then repeating this process an arbitrarily large number of times and averaging the results (Sobol 1974).

Although Monte Carlo simulation is able to solve deterministic models, such as the value of a definite integral, one of its important uses is solving stochastic models; that is, models that have a random element (Rubenstein 1981). The method is most effective for solving problems where

the result only needs to be accurate to within 5-10% (Sobol 1974). The use of a method for solving models with a random element is a powerful tool in hydrology, as many components of a hydrologic system have inherent randomness. The technique has been used within hydrology to study flood frequency analysis (Rahman et al. 2002 and Loukas 2002), rainfall-runoff modeling (Marshall et al. 2004), uncertainty analysis for climate change scenarios (New and Hulme 2000), climate change impacts on combined sewer performance (Kleidorfer et al. 2009), and low-flow scenarios for streamflow (Wilby and Harris 2006), among others. The important component common to all of these studies is the quantification of uncertainty by use of statistical methods and stochastic modeling.

The study described by Wilby and Harris (2006) served as a framework for establishing a model for handling uncertainties in projecting streamflow in a changing climate. The authors combined the projections of four global climate models, two greenhouse gas emissions scenarios, two climate data downscaling techniques, two hydrologic models, and two sets of hydrologic model parameters in order to assess the frequency of low-flow events for the Thames River in the United Kingdom. By describing the probability of occurrence of the components in the stochastic system, a weighted result based on these probabilities can be used to improve predictions of the low-flow parameter (in this case Q_{95}, the average streamflow exceeded on 95% of days in a year).

Following the framework presented by Wilby and Harris (2006), we sought to describe the sources of uncertainty in projecting runoff generated by common design storms in a changing climate, as well as to use Monte Carlo simulation to improve the estimate of runoff in the

future. The random variables chosen to be modeled are from two categories: future climate uncertainty and hydrologic model uncertainty.

The uncertainty in future climate was assessed by comparing results from two greenhouse gas emissions "storylines" and nine to ten GCMs per emissions scenario. The data were downscaled using the hybrid delta method (Hamlet et al. 2010), which is a combination of bias correction and delta change. However, the hybrid delta downscaling method is not a transient method. The GCM simulations are bias-corrected at the coarse GCM resolution by comparing GCM historical runs to observed historical data that have been gridded to the GCM resolution. The perturbed monthly values are then projected on to a 1915-2006 historical daily time series creating daily downscaled meteorological data, which produces 92 realizations of a future climate for a 30-year period surrounding 2045. Because the GCMs were projecting a climate for the mid 21st century, the selected emissions scenarios (A1B and B1) represent the "worst" and "best" case scenarios for that time period (Mote and Salathé 2010). Each GCM was evaluated for its ability to reproduce the precipitation and temperature of the Pacific Northwest for the historical period of 1970-1999 by Mote and Salathé (2010).

Because the soil-related model parameters were calibrated for a 1/16 degree resolution model set-up and were then aggregated to 1/2 degree, and computational limitations made it difficult to test the uncertainty in soil parameters, the uncertainty contained within the hydrology model was handled differently than the study by Wilby and Harris (2006). The authors used a regression-based catchment model and manually changed five parameters affecting evaporation, percolation and storage for each zone contributing to the catchment area, resulting

in different runoff regimes. Instead, we addressed the uncertainty in the hydrology model in terms of two factors contributing to the magnitude of runoff events: antecedent soil moisture and snowpack. Antecedent soil moisture and snowpack can change the amount of runoff produced in a precipitation event. For soil moisture, common infiltration-runoff calculation methods such as the SCS "curve number" method (USDA 1986), Horton equation or the Green-Ampt method consider the amount of soil moisture present when determining the amount and rate of infiltration and runoff (Chow et al. 1988, Bedient et al. 2008).

The infiltration and runoff behavior of soils in temperate, moist zones is different from that of semi-arid areas (Wei et al. 2007). This is important considering the difference between the moist maritime zones west of the Cascade Mountains and the rain shadow desert and continental climate of eastern Washington and Oregon. Antecedent soil moisture conditions are important in controlling runoff during low to mid-intensity storms and are a major factor in the hydrology of semiarid areas (Castillo et al. 2003). Antecedent snowpack conditions can also affect the runoff output of an extreme rainfall event, such as the 1996 Pacific Northwest flood (Marks et al. 1998, Marks et al. 2001). Existing snowpack can add a significant water input to a system when weather conditions accelerate deterioration through processes that add energy to the snowpack such as increased boundary layer turbulence from increased wind speed and advection from precipitation (Marks et al. 2001, Dingman 2002).

To include the effects of these processes into the modeling, VIC was run for a period of 1957-1989 for the historical climate and for the 1957-1989 period that has been perturbed to represent the 2040s climate for each emissions scenario and GCM. The three-layer soil

moistures and the snowpack for the date indicated by peak occurrence of the annual maximum precipitation event were sampled, treating 1957-1959 as spin-up years to set realistic soil moisture values within the model prior to sampling. These years were approximately neutral in relation to the Pacific Decadal Oscillation, and only late 1957 was an El Niño event (Mantua and Hare 2002, Cane et al. 1986). The soil moisture for the three layers and the snowpack were fit to a normal distribution using the method of moments. The fit for snow water-equivalent is shown in figure 4 for a sample grid cell by comparison of empirical and distribution-fit quantile functions. The distribution was then discretized to three bins as shown in Table 1. This creates a finite number of combinations to reduce the number of required simulations and to prevent negative values for soil moisture and snow water-equivalent when initializing the hydrology model. Negative values can occur for small percentiles of the normal distribution because the distribution has no lower bound preventing negative values. A comparison of continuous and discrete distributions for a sample grid cell is in figure 4. A spin-up state file (a starting point of model state) for each climate scenario was created for each combination of discrete snowpack and 3-layer soil moisture quantiles. This created a way of controlling the initial conditions for the hydrologic simulation for each storm event in terms of the likelihood of the soil moisture and snow water-equivalent.

Because there is no analytical solution of the quantile function for the normal distribution, a fast approximation by Voutier (2010) was used to generate the quantile values. For $0.025 \leq p \leq 0.975$ the approximation has a maximum absolute error less than 1.16×10^{-4}.

Table 1: Bins for discretizing normal distribution of 3-layer soil moisture and snow water-equivalent values. The discrete quantile function is shown in figure 4 with the continuous quantile function. All values for the quantile function were returned as the greater of the function or zero.

Continuous Probabilities	Discrete Probability
0.00 – 0.25	0.125
0.25 – 0.75	0.5
0.75 – 1.00	0.875

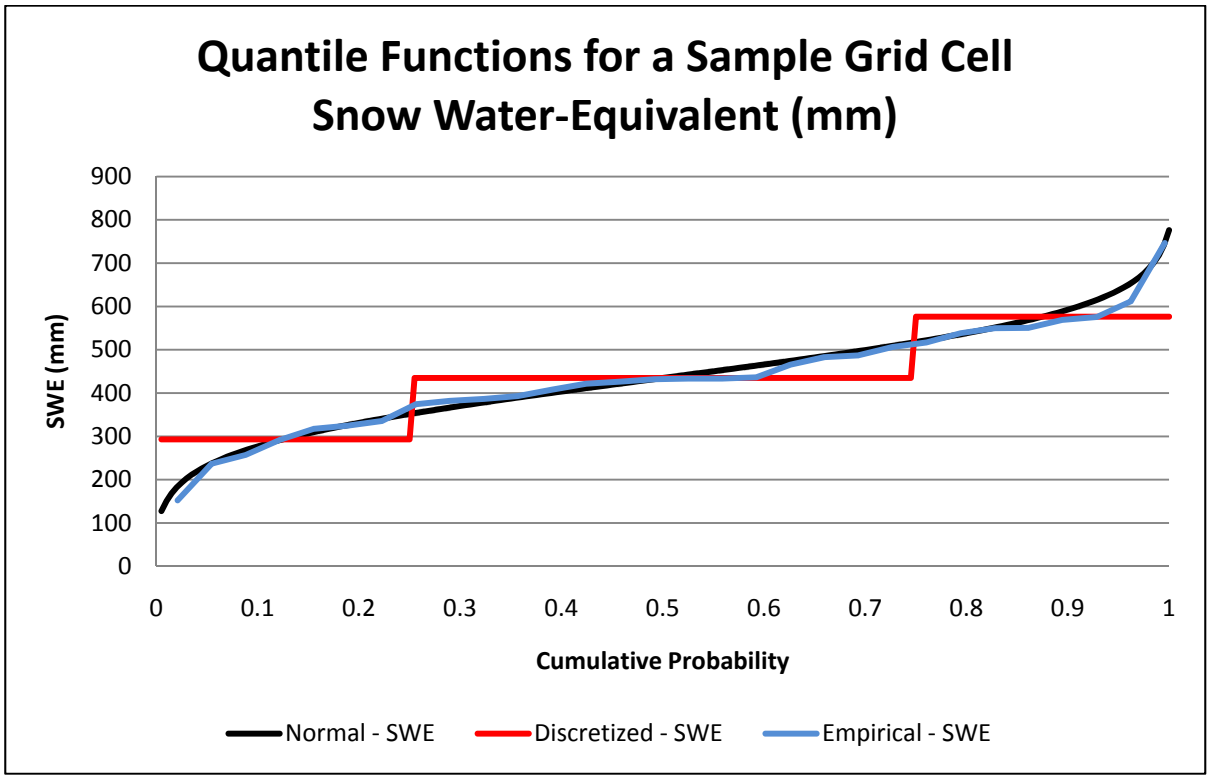

Figure 4: Continuous, discrete and empirical quantile functions for snow water-equivalent in a sample grid cell within the domain. The discrete function comes from the bins in table 1. The empirical function was assigned a probability using the Blom plotting position for ranked data. The quantile functions were generated using the fast quantile approximation by Voutier (2010) which has a maximum absolute error of less than 1.16 x 10^{-4} for $0.025 \leq p \leq 0.975$.

To determine a weighting scheme for the Monte Carlo process, each component of uncertainty needed to have a probabilistic model governing its selection. This was done either by assessing the quality of the predictor, in the case of the GCM, or by a distribution fit, in the case of antecedent soil moisture and snowpack.

To select an emissions scenario based on the probability of the actual occurrence of that storyline, assumptions about the world economy and other grand assumptions outside of the scope of this study would have to be made (Wilby and Harris 2006). There is currently no universally accepted way to predict the occurrence of an emissions storyline in the future (Nakićenović and Swart 2000), so each scenario (A1B and B1) was given equal probability of occurrence (p = 0.5) as in Giorgi and Mearns (2003).

The probability of selection for each GCM was based on the performance of each model in hindcasting the 1970-1999 Pacific Northwest climate as per the results in the study by Mote and Salathé (2010). Each model was weighted by its average annual temperature and monthly precipitation bias compared to the University of East Anglia Climate Research Unit (CRU) version 2.02 half-degree grid data (Mitchell et al. 2004), over the evaluation period, and the models with a lower average bias were given a higher probability of selection. Table 2 shows the probability of each respective model in terms of its average temperature and precipitation bias. Because downscaled data for the HADGEM1 model were only available for the A1B emissions scenario, the individual probability of each model for the two emissions scenarios is different. The probability for each model is proportional to the inverse of the Pythagorean addition of the average biases (equation 6).

$$P_i = \frac{C_{es}}{\sqrt{Bias_{T,i}^2 + Bias_{P,i}^2}} \tag{6}$$

The constant of proportion is dependent on the emissions scenario in order to force the sum of the probabilities equal to unity, shown in table 3. The constant differs due to the different number of GCMs present for each emissions scenario. This model for probability was based on the distance each model is from the origin, or zero average bias, on the plot in figure 5.

Table 2: GCM selection probabilities from equation 6. The bias for each model is for backcasted 1970-1999 climate as determined by Mote and Salathé (2010). The citation for each model can be found in table 8.1 of Randall et al. (2007). The constant in equation 6 is dependent on the emissions scenario and is shown in table 3. The constants are to make the sum of the probability of selecting the GCMs equal to unity.

GCM	Average Annual T Bias (°C)	Average Monthly P Bias (cm)	A1B P	B1 P
CCSM3	-1.7	1.8	0.107	0.118
CGCM3.1_t47	-2.3	1.7	0.093	0.102
CNRM_CM3	-0.8	1.7	0.141	0.155
ECHAM5	-1.8	1.7	0.107	0.118
ECHO_G	-2.2	1.7	0.095	0.105
HADCM	-1.9	1.3	0.115	0.127
HADGEM1	-1.8	2.2	0.093	--*
IPSL_CM4	-1.6	2.4	0.092	0.101
MIROC_3.2	-1.5	3.2	0.075	0.083
PCM1	-2.8	1.6	0.082	0.091
	Average: -1.8	**Average: 1.9**	**Sum: 1.000**	**Sum: 1.000**

*There were no downscaled data available for HADGEM1 running B1.

Table 3: Proportionality constants (Ces) for equation 6 which make the sum of the selection probabilities for the GCMs equal to unity, as shown in table 2.

Emissions Scenario	Constant
A1B	0.26488
B1	0.29210

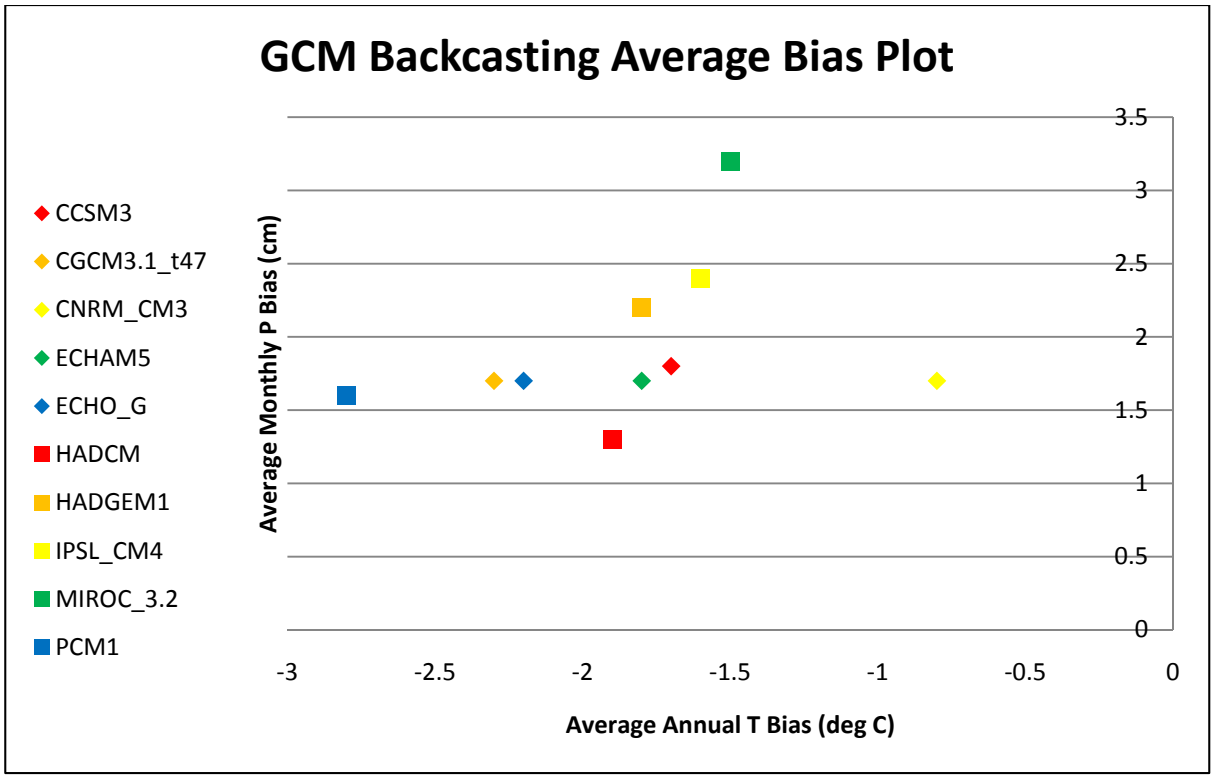

Figure 5: Plot of biases for the 10 GCMs in the study. The average annual temperature bias for the model in hindcasting the 1970-1999 climate is on the x-axis and the average monthly precipitation bias is on the y-axis. The probability of selecting the GCM is based on the distance the model is from the origin, which is equivalent to zero average bias.

The selection of each soil moisture and snowpack percentile was based on the discretized normal distribution as defined in table 1. Instead of generating Gaussian random values, an approximate distribution with a lower bound at zero having discrete probabilities was applied and quantiles were selected by selecting probabilities from a uniform distribution on (0,1). These values were selected independently, as for the majority of grid cells in the PNW there was not a significant correlation between soil moisture in any of the three soil layers and SWE.

For each ARI, a combination of emissions scenario, GCM, soil moisture percentile and snow water-equivalent percentile were selected at random 5000 times using a pseudorandom number

generator and the probability distribution of each variable. The pseudorandom number generator of choice is the "Mersenne Twister", a fast and portable generator ideal for Monte Carlo simulation (Matsumoto and Nishimura 1998). The result of the Monte Carlo selection scheme was used to "weight" these results for a probabilistic outcome to determine a median outcome as well as a probable range for the results. The complete set of results is also used to isolate individual causes of uncertainty and variability in predicting the future climate. The method for selecting a scenario is shown for one selection in figure 6.

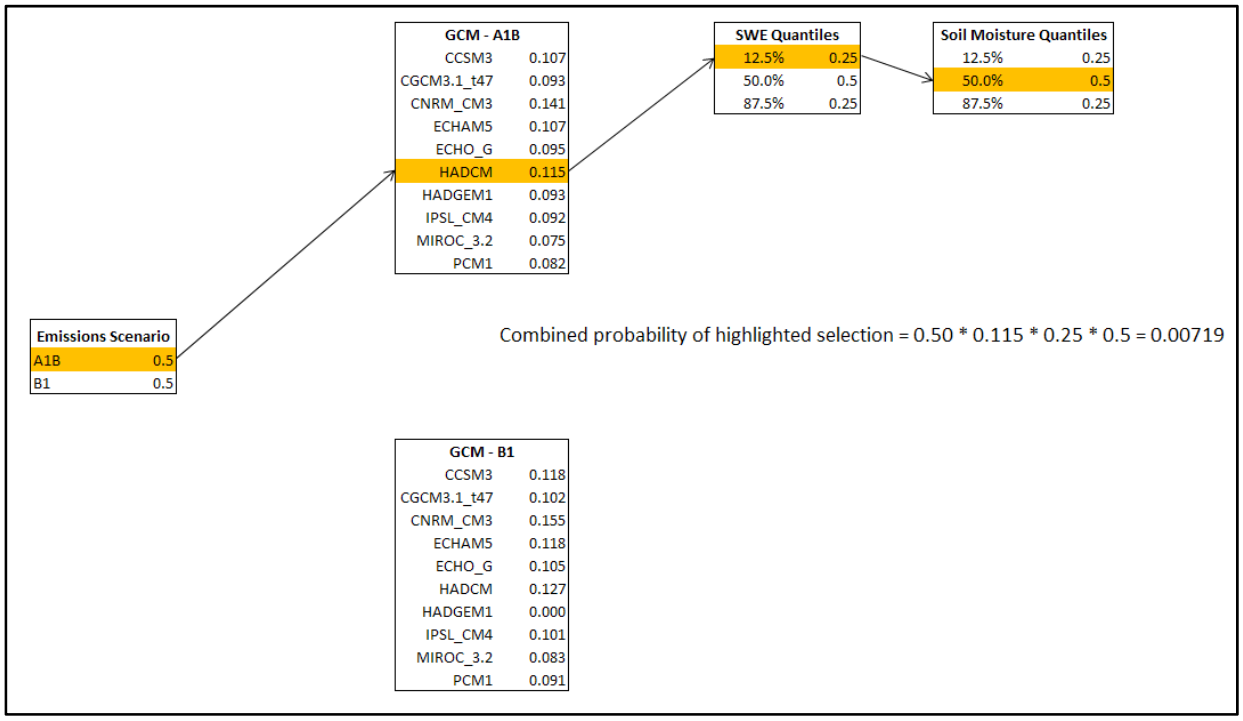

Figure 6: Illustration of one realization of random selection for emissions scenario, GCM, SWE quantile and snowpack quantile

3. Results

As related to the two research questions described in chapter 1, the two major components of analysis presented herein are the probabilistic forecasts created by the Monte Carlo simulation, and a comparative analysis of the respective factors contributing to uncertainty in the probabilistic forecast. The forecast is compared to historical simulations of runoff for a precipitation event of equivalent ARI. The historical storm events were modeled with three discrete states of initial snowpack and soil moisture in the same way that the future climate scenarios were modeled. Because the parameters were drawn from discrete distributions for the snowpack and soil moisture quantiles, the results are not continuous as there are a finite number of combinations. The range of uncertainty will be presented in terms of the coefficient of variation for the sampled 5000 realizations along with the mean event.

3.1 24-Hour Design Storm Intensities

The 50-year storm is being presented here as a significant design extreme event with an ARI shorter than the length of record (1915-2006; 92 years). The 25-year or 100-year storm could have alternatively been shown; however, the use of the most extreme event within the length of record that was modeled was chosen for illustration. The 2, 25 and 100-year 24-hour storm intensities are illustrated in the appendix (section A.1).

The intensity of the historical 50-year 24-hour storm is shown in figure 7, generated from the GEV distribution quantile function fit by the method of L-moments. The L-moment sample

parameters, with the selected GEV model, are shown for illustration in the appendix (section A.3).

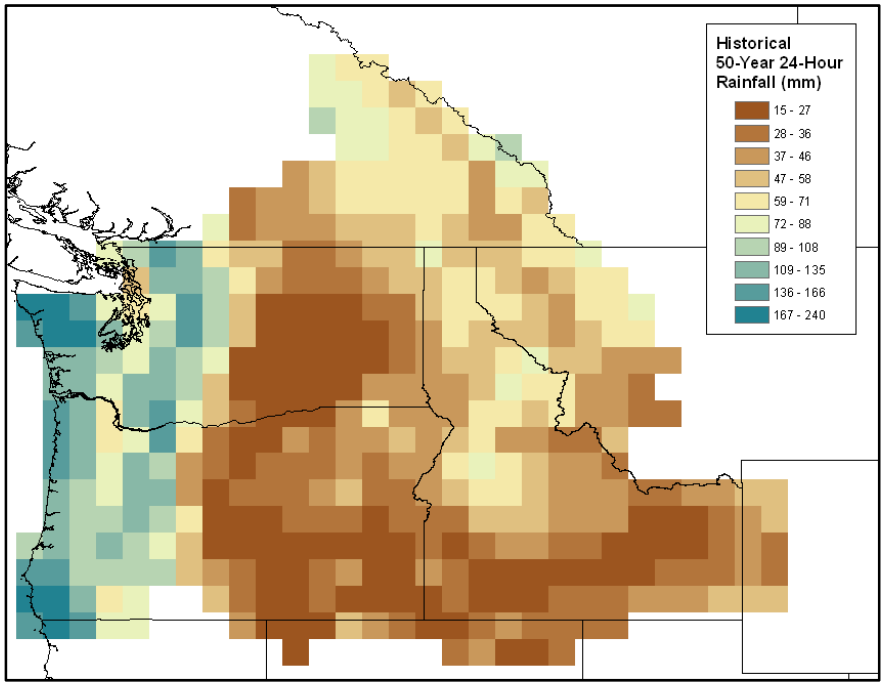

Figure 7: Historical 50-year 24-hour storm intensity in millimeters as determined by the GEV distribution quantile function fit to the annual maximum rainfall event series for 1/2 degree meteorological data aggregated from Elsner et al. (2010) 1/16 degree meteorological data.

In comparison, a sample GCM/emissions scenario pair (CNRM CM3 running the B1 emissions scenario) is shown in figure 8 below. CNRM CM3 is the model with the highest selection in table 2. For the majority of the domain, the intensity of the 50-year 24-hour storm increased for this scenario, with a mean change of +8.6%. 185 of 425 cells (43.5%) resulted in a change of greater than or equal to +10%. 78 of 425 cells (18.3%) resulted in a decrease in intensity, with a largest decrease of -17.3%. 67% of the cells projected to decrease in intensity were reduced by less than or equal to 5%.

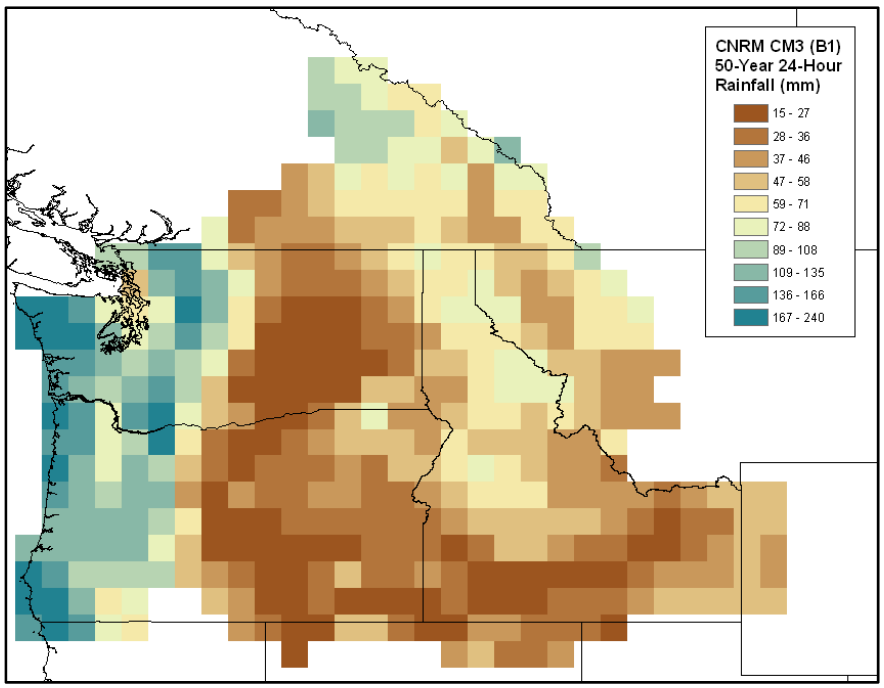

Figure 8: Future 50-year 24-hour storm intensity in millimeters; determined by the GEV distribution quantile function fit to the annual maximum rainfall event series for 1/2 degree meteorological data aggregated from 1/16 degree downscaled data from CNRM CM3 running the B1 emissions scenario.

3.2 Synthetic Meteorological Data

The synthesized meteorological data used for driving VIC in event mode were created by the averaging of daily minimum and maximum temperature and average wind speed for the two-week period with the highest relative frequency for annual maximum rainfall event for each grid cell. The average temperature for the historical and future (CNRM CM3/B1) and historical wind speeds are shown in figure 9. For the future climate, average daily wind speeds are randomly sampled from the historical data (Wood et al. 2002). Both T_{min} and T_{max} values increased on average in the future case, as would be expected by use of a delta downscaling method.

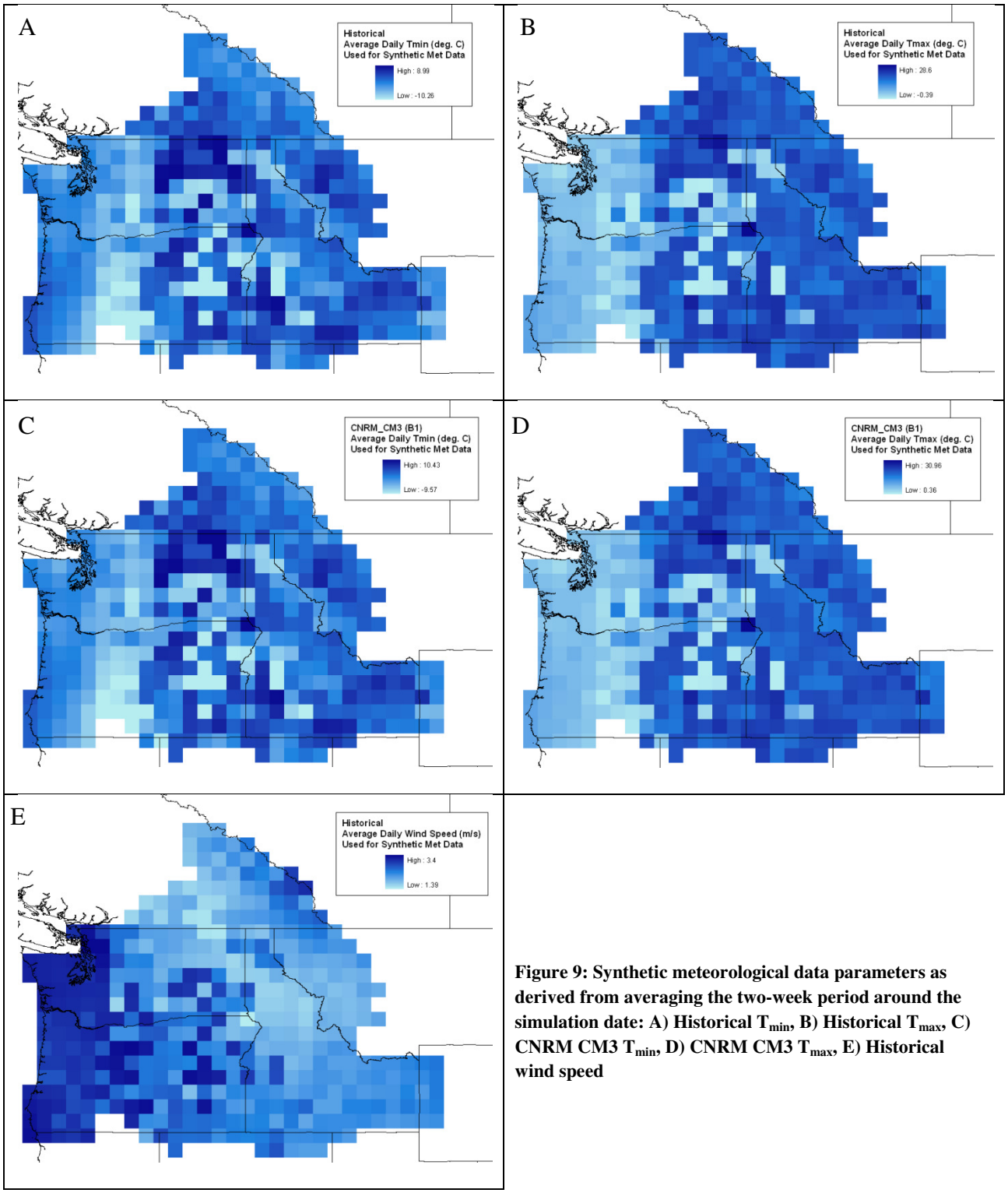

Figure 9: Synthetic meteorological data parameters as derived from averaging the two-week period around the simulation date: A) Historical T_{min}, B) Historical T_{max}, C) CNRM CM3 T_{min}, D) CNRM CM3 T_{max}, E) Historical wind speed

3.3 Snow Water-Equivalent and Soil Moisture

The resulting median snow water-equivalent and top-layer soil moisture for the historical period and a selected climate scenario (CNRM CM3 running B1) are shown in figure 10. These values are derived from a discretized normal distribution (see table 1 and figure 4) fit to 30 years of VIC-simulated snow water-equivalent and soil moisture. The values were taken for the date at the center of the two-week climate averaging window determined in section 2.4.2. The grid-averaged top-layer soil moisture remained constant between the historical and GCM-simulated results (23.00 mm and 22.78 mm respectively) but snow water-equivalent decreased from a grid-average 9.16 mm to 5.95 mm. In even warmer cases, due to emissions scenario or model with a warmer hindcasting bias, the snowpack decreased even more from the historical case.

3.4 Monte Carlo Probabilistic Forecasts

The runoff simulation results for the 50-year storm are presented here; the other ARI storm results (for the 2, 25, and 100-year storms) are included in the appendix (A.1). Future runoff conditions followed the same spatial pattern as the historical runoff. Figure 11 illustrates the runoff depth for the 50-year storm for the Monte Carlo averaged historical event, and figure 12 shows the result of the Monte Carlo simulation for the 2040s. While the spatial signature on these plots is clear and reflects the established precipitation regimes of the Pacific Northwest, the plot of the percent change from historical to future has a weaker signal, as shown in figure 13. In general, the northern and eastern regions of the domain show zero to negative changes, with increasing values to the south and west. Changes were not strongly reflective of the

historical precipitation regimes, with both wet and dry areas showing positive and negative change, but generally wetter regions (in the western part of the domain) showed increases in runoff. It is clear that on average in the Pacific Northwest the amount of runoff is increasing in a changing climate, which is indicated by a majority of grid cells in the domain having at least a 5% increase in runoff in the 2040s simulation for the 50-year storm.

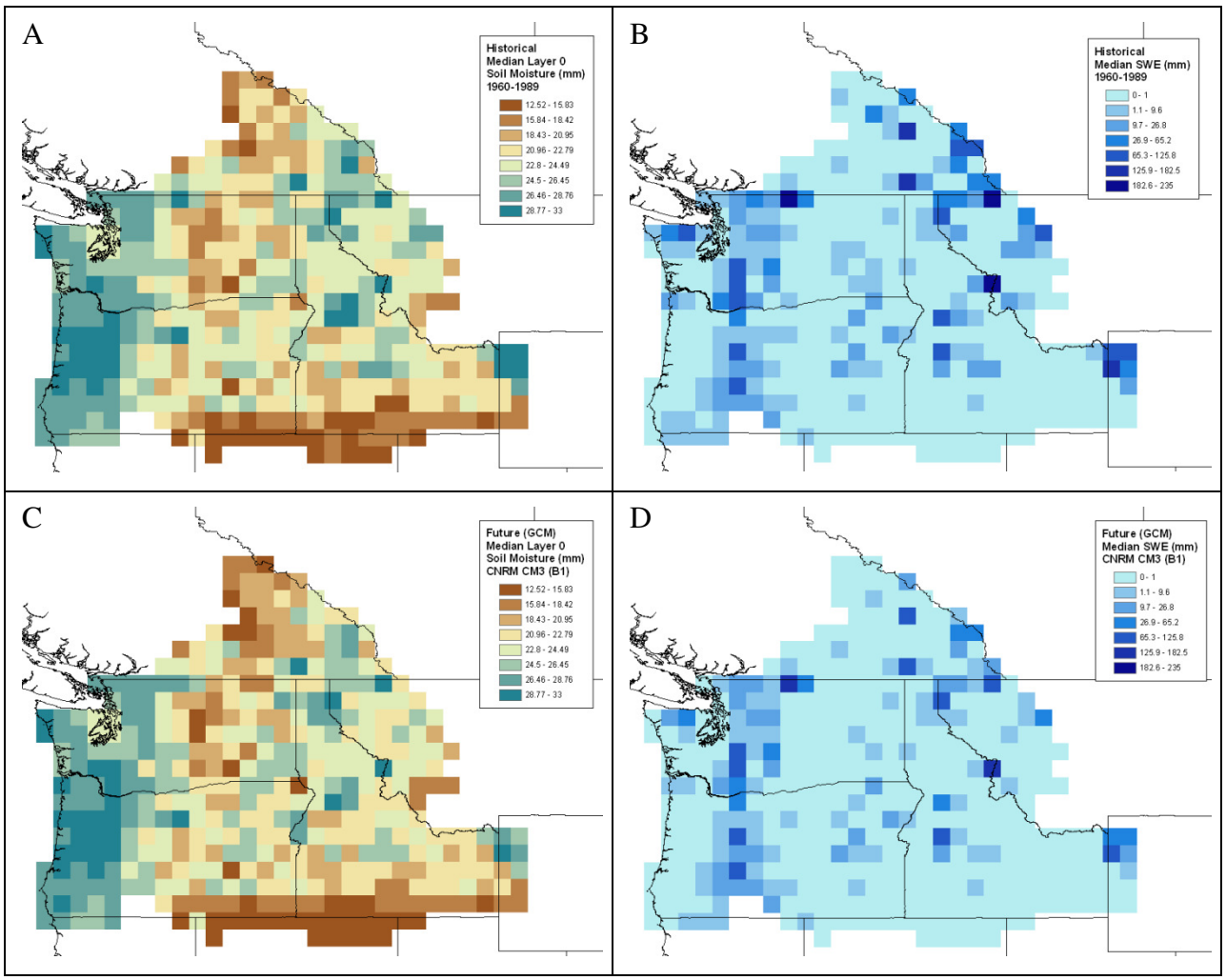

Figure 10: Median A) historical top-layer soil moisture, B) Historical median snow water-equivalent, C) CNRM CM3 (B1) top-layer soil moisture and D) CNRM CM3 (B1) snow water-equivalent (in mm) for 1960-1989 (historical) and 2040s climate (future) at the simulation date selected in section 2.4.2. Values were derived from a discretized version of the fast quantile approximation for the normal distribution in Voutier (2010) for the 30-year sample.

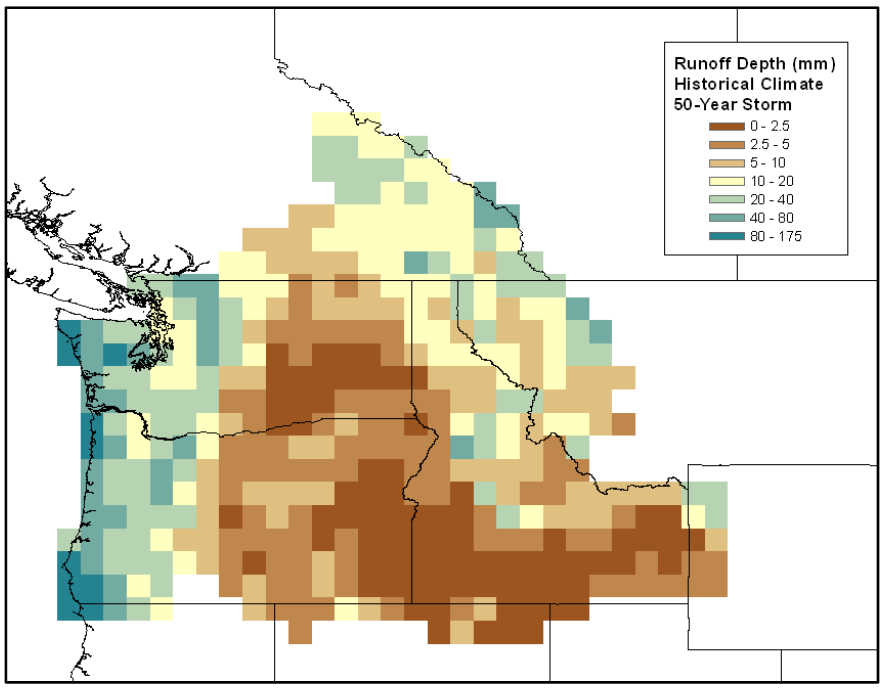

Figure 11: Runoff depth in millimeters for the historical 50-year storm with random selection of soil moisture and snow water-equivalent quantile.

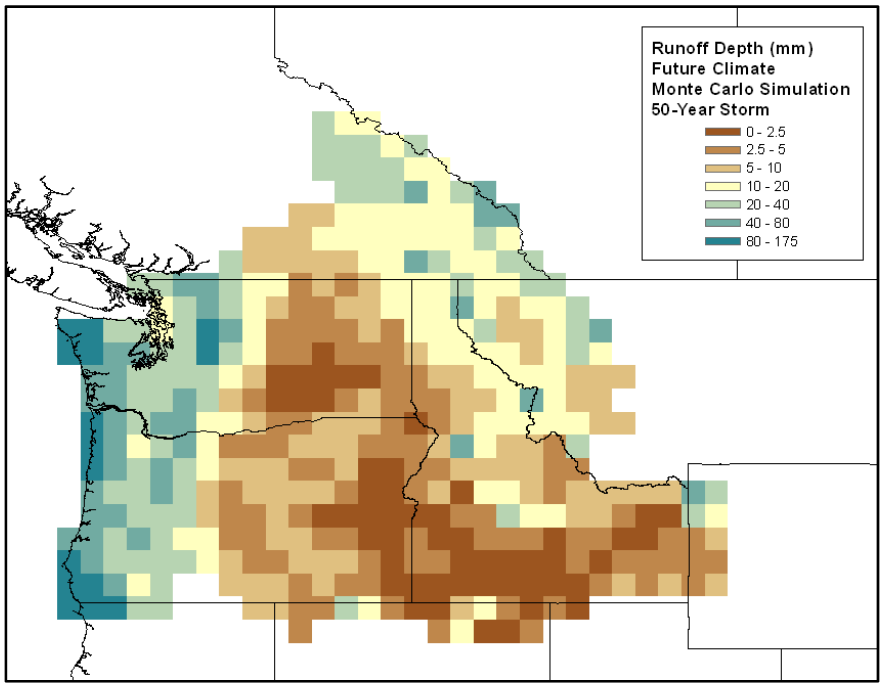

Figure 12: Runoff depth in millimeters for the future 50-year storm with 5000 realizations of random selections of emissions scenario, GCM, soil quantile, and snow quantile

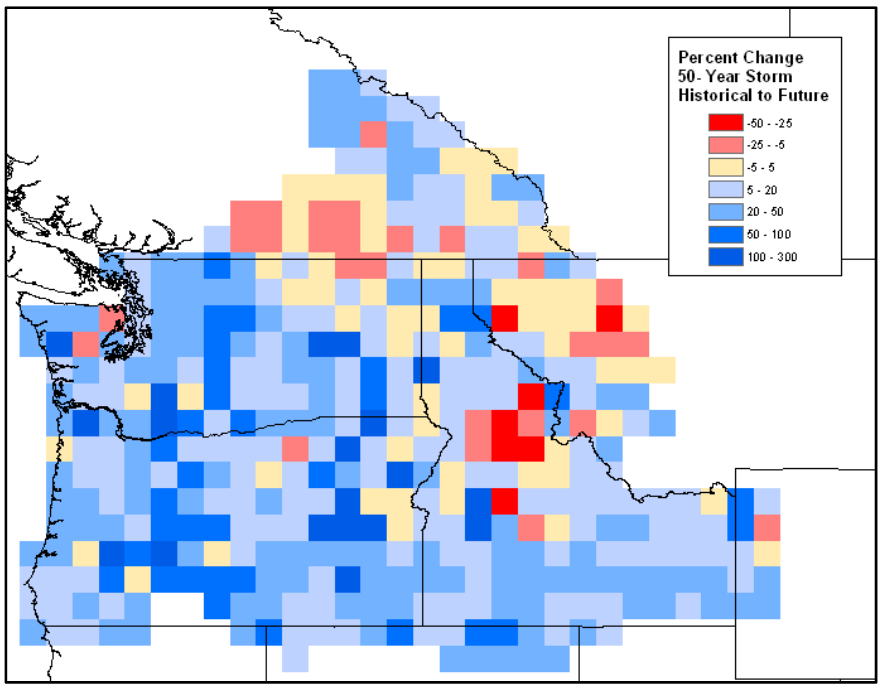

Figure 13: Percent change for the historical and future runoff depth for the 50-year storm, calculated as the percent change from figure 11 to figure 12.

It is also important to consider the range of possibilities that were generated by the various combinations of parameters being tested. Because of the discrete distributions employed for selecting all uncertainty parameters (emissions scenario, GCM, antecedent soil moisture and antecedent snowpack), there are a finite number of "chains" that can occur by random selection. If the four parameters with the lowest selection probability are chosen for a random selection, the minimum combined probability of that selection is about 0.23%. This is the combination of probabilities for the selection of all the least frequent events. This means that in 5000 realizations these 'rare' events are expected to occur about 11 times.

Figure 14 shows, as a percent change from the historical storm event, the largest simulated runoff event of 5000 realizations for each grid cell due to the 50-year storm. The three

scenarios that caused the largest grid-average change in runoff are shown in table 4. In general, the causes of increased simulated runoff results were higher greenhouse gas emissions, a GCM with a warmer temperature hindcasting bias and a wetter precipitation hindcasting bias, lower snow water-equivalent, and higher soil moisture. The three largest runoff averages occurred with MIROC 3.2 climate projections. From table 2, MIROC 3.2 is the "wettest" GCM in regard to hindcasting precipitation bias (MIROC 3.2 = 3.2 cm/mo, GCM average = 1.9 cm/mo), and the second warmest in temperature bias (MIROC 3.2 = -1.5 °C/yr, GCM average = -1.8 °C/yr), as well as having the lowest probability of selection for the Monte Carlo simulation. The largest events feature runoff depths as high as a twentyfold increase in one location in western Idaho, and several cells in eastern Washington and Oregon and northern Nevada resulted in more than 400% of the historical runoff depth. The locations with the largest increases would seem to indicate the areas that have the most sensitivity to the uncertainty analysis parameters.

However, these locations typically have only a small amount of precipitation and low runoff depths. The cell in western Idaho with the twentyfold increase, for example, only resulted in a 1.21 mm runoff depth for the 50-year storm in the Monte Carlo simulation for future climate and a weighted average of only 0.31 mm for the historical scenario. Areas that experienced significant runoff in the historical and future simulations as well as experiencing a large possible increase in the largest simulated event, such as the Olympic Peninsula, could be at a significant risk in terms of runoff, as will be discussed later.

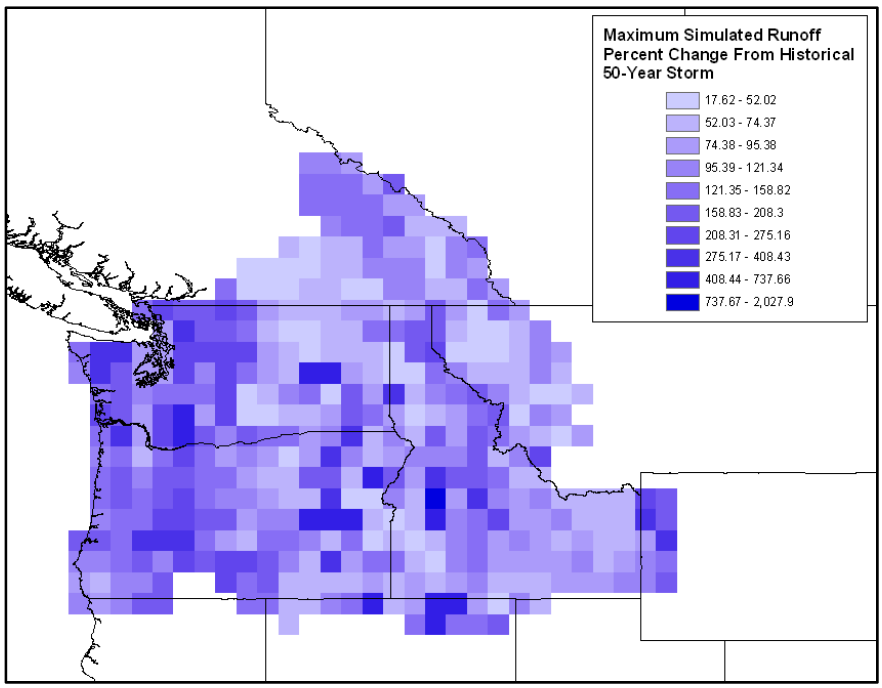

Figure 14: Percent change from the runoff depth due to the historical 50-year storm to the largest grid-average runoff depth that occurred in 5000 realizations of Monte Carlo simulation for the future 50-year storm

Table 4: Combinations of emissions scenario, GCM, snow water-equivalent quantile and soil moisture quantile resulting in the three largest 425-cell averaged runoff for the 50-year event

Rank (Largest)	Emissions Scenario	GCM	Snow Quantile	Soil Moisture Quantile
1	A1B	MIROC 3.2	12.5%	87.5%
2	A1B	MIROC 3.2	50%	87.5%
3	B1	MIROC 3.2	12.5%	87.5%

At the other extreme, the minimum simulated event in 5000 realizations represents the combination of parameters that limits runoff the most. In general this was related to a lower greenhouse gas emissions scenario, a GCM with a lower precipitation bias and a cooler temperature bias, higher snow water-equivalent, and lower soil moisture. Table 5 shows the three smallest runoff events by grid average. As in the results for the largest event, one GCM was responsible for the three smallest runoff events. The ECHO G model, as shown in table 2,

had the 3rd coldest hindcasting temperature bias (ECHO G = -2.2 °C/yr, GCM average = -1.8 °C/yr) and was tied for 2nd driest for precipitation bias (ECHO G = 1.7 cm/mo, GCM average = 1.9 cm/mo). It ranked fifth among the ten models in selection probability for the Monte Carlo Simulation. The magnitude of these changes are much smaller than those presented in the maximum case, tending toward a mean value of about -37%, and are bounded below by a value of zero runoff where all precipitation is either infiltrated or captured by snowpack (where the maximum case is bounded above by the total water input coming from precipitation and melting snowpack, and infiltration is minimal). Figure 15 shows the distribution of the changes in runoff from the historical to the minimum simulated 50-year storm. For the minimum simulated event, most areas experience decreases, and the areas experiencing the greatest decrease in runoff depth are in the coastal areas of Washington and Oregon, and the higher elevations in the interior of Idaho. Due to the combination of conditions, some locations, particularly in western Washington and Oregon, resulted in zero runoff in the minimum case.

However, there are locations in the domain that, even in the case of the minimum simulated future runoff, still feature an increase from the historical runoff due to the 50-year storm. Locations displaying this behavior have the highest probability of experiencing increased runoff in the future. Two of these locations are at low risk (with projected runoff less than 4 mm) however, one location on the Washington-British Columbia border projects a minimum change of +3.08% for the 50-year storm with a Monte Carlo forecasted value of 21.15 mm.

Table 5: Combinations of emissions scenario, GCM, snow water-equivalent quantile and soil moisture quantile resulting in the three smallest 425-cell averaged runoff for the 50-year event

Rank (Smallest)	Emissions Scenario	GCM	Snow Quantile	Soil Moisture Quantile
1	B1	ECHO G	87.5%	12.5%
2	B1	ECHO G	50%	12.5%
3	A1B	ECHO G	87.5%	12.5%

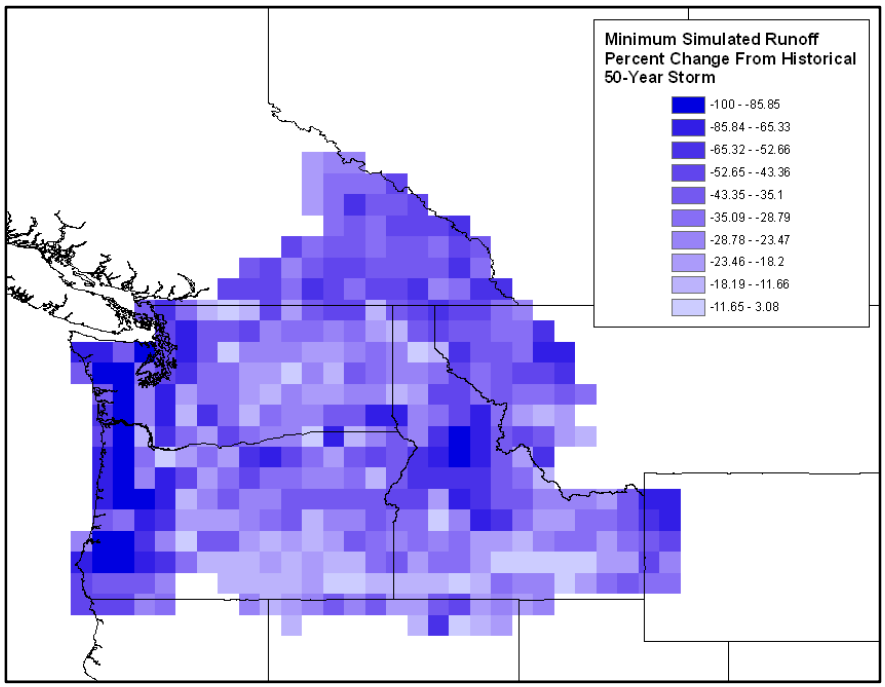

Figure 15: Percent change from the runoff depth due to the historical 50-year storm to the minimum runoff depth in 5000 realizations of Monte Carlo simulation of the runoff depth due to the future 50-year storm. A -100% change indicates zero runoff as a minimum case.

In figure 16, the coefficient of variation (CV) for the 5000 simulated values is presented. The coefficient of variation for each cell is defined in equation 7 in terms of the standard deviation σ and the mean μ of the simulated values. This represents the overall uncertainty in prediction due to selection of all four parameters for the runoff regimes for the domain. Two regions have a large uncertainty, the higher elevation region of central Idaho, and the wet western side of the

Cascade Mountains in Washington and Oregon. Areas with a lower CV were dryer areas where mean runoff is generally small and less variable.

$$CV = \frac{\sigma}{\mu} \tag{7}$$

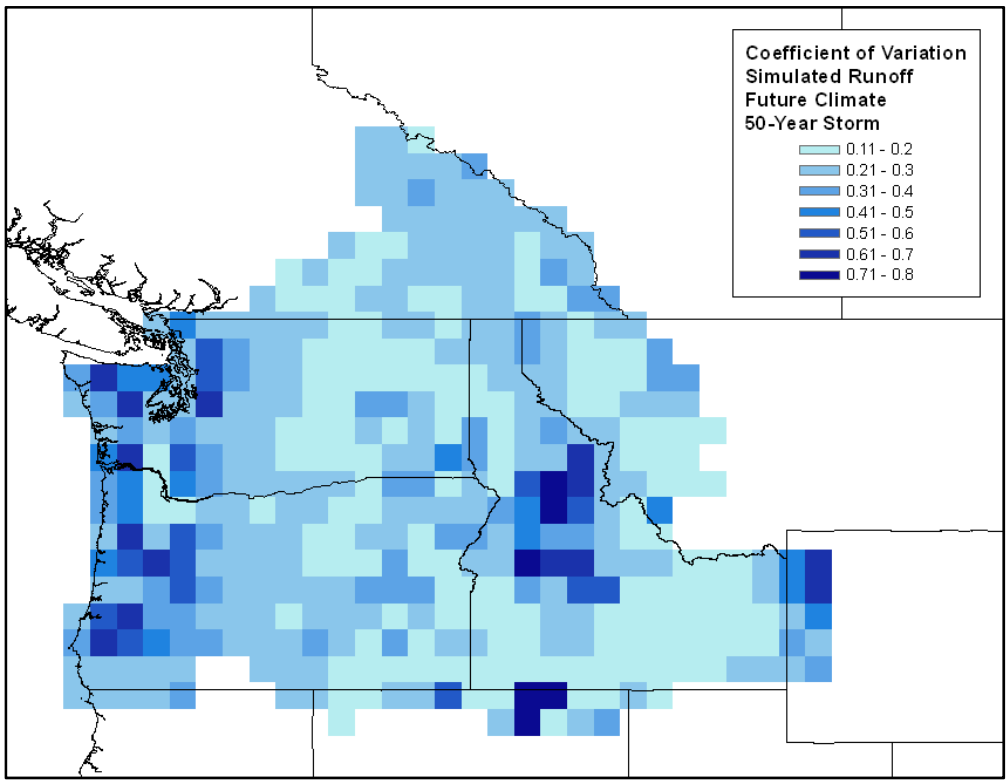

Figure 16: Coefficient of variation for 5000 realizations of simulated runoff depth for the future 50-year storm.

The results of the Monte Carlo simulation for each grid cell were fit to a normal distribution using the method of moments in order to create confidence intervals for runoff at that location for the future 50-year storm. Figure 17 shows the 10% and 90% runoff depths for the 50-year storm. Note that one grid cell resulted in a negative runoff depth, which is due to the normal distribution having no lower bound preventing negative values.

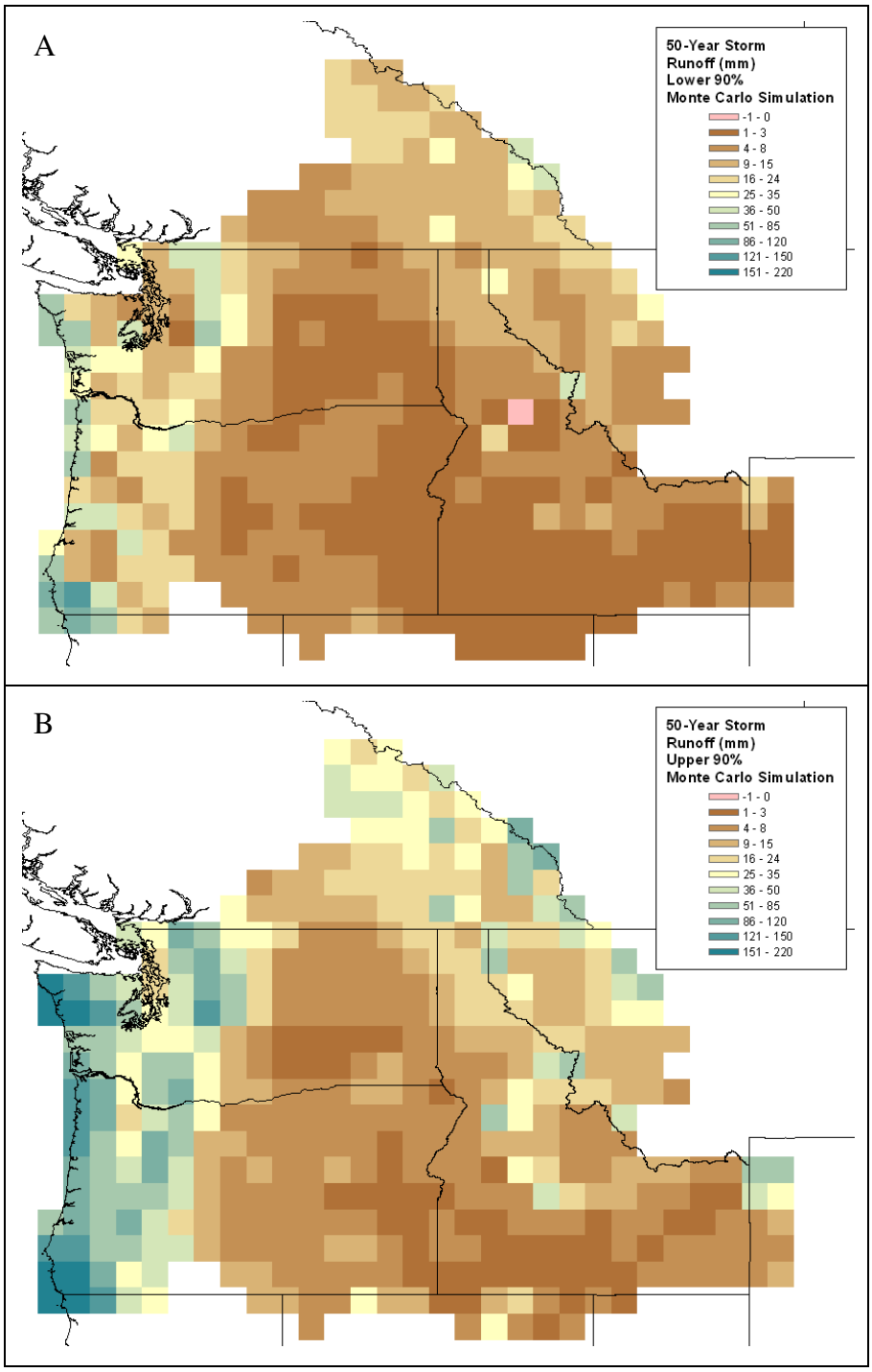

Figure 17: 90% confidence interval for runoff due to the future 50-year storm from the Monte Carlo simulation. A) 10% runoff depth (lower bound), B) 90% runoff depth (upper bound)

Additionally, for two representative grid cells in the domain, cumulative distribution functions (CDFs) were constructed to show the posterior distribution of these results. For each, a CDF for the historical results, the future results, and the change between the two is shown. Figure 18 locates the two sample grid cells in the domain. Figure 19 is for the grid cell over the Queets River basin on the western Olympic Peninsula, and figure 20 is for the grid cell over the Palouse River basin in eastern Washington and western Idaho.

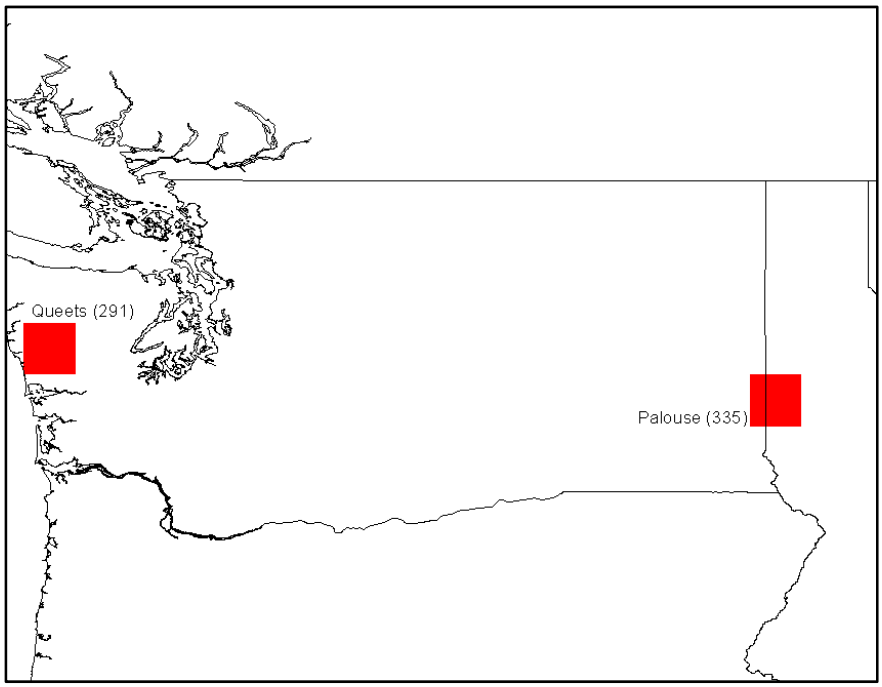

Figure 18: Location of half-degree grid cells over the Queets River and Palouse River basins in the Pacific Northwest.

The CDFs illustrate the distinctly different runoff regimes between the two cells, and the amount of variability present in the estimate for the change in runoff in the two locations. These CDFs can be used to represent the amount of uncertainty in projecting runoff for an individual location.

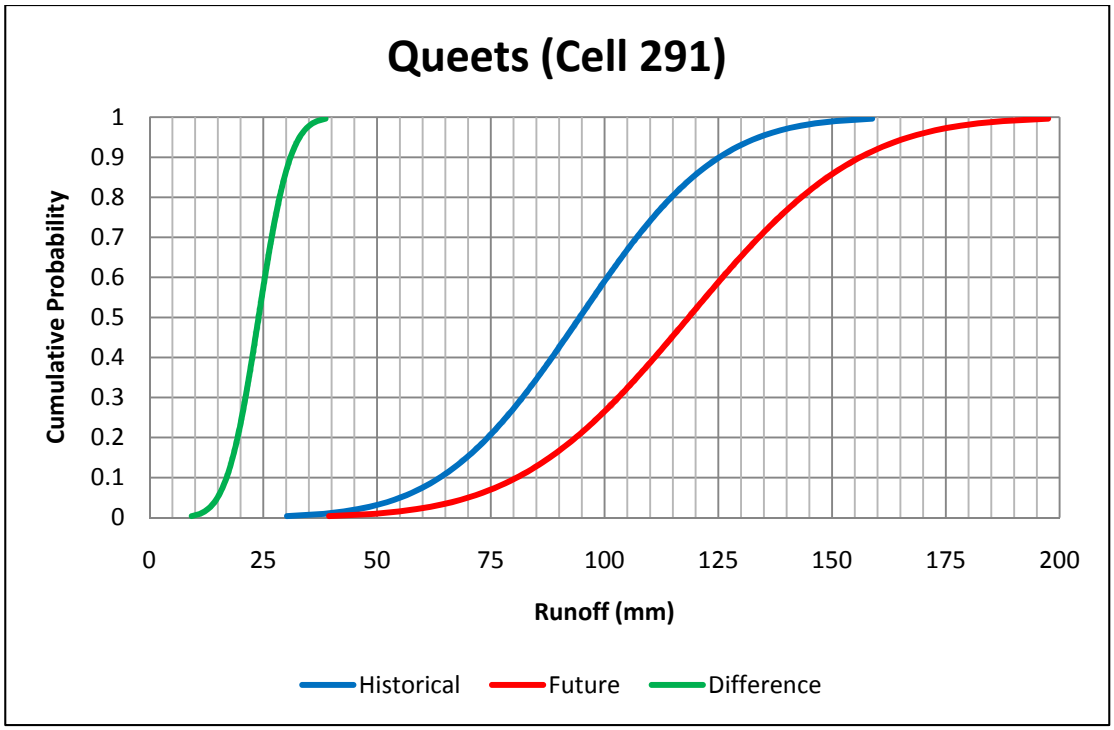

Figure 19: Historical, future and difference 50-year storm runoff CDFs for the grid cell over the Queets River basin

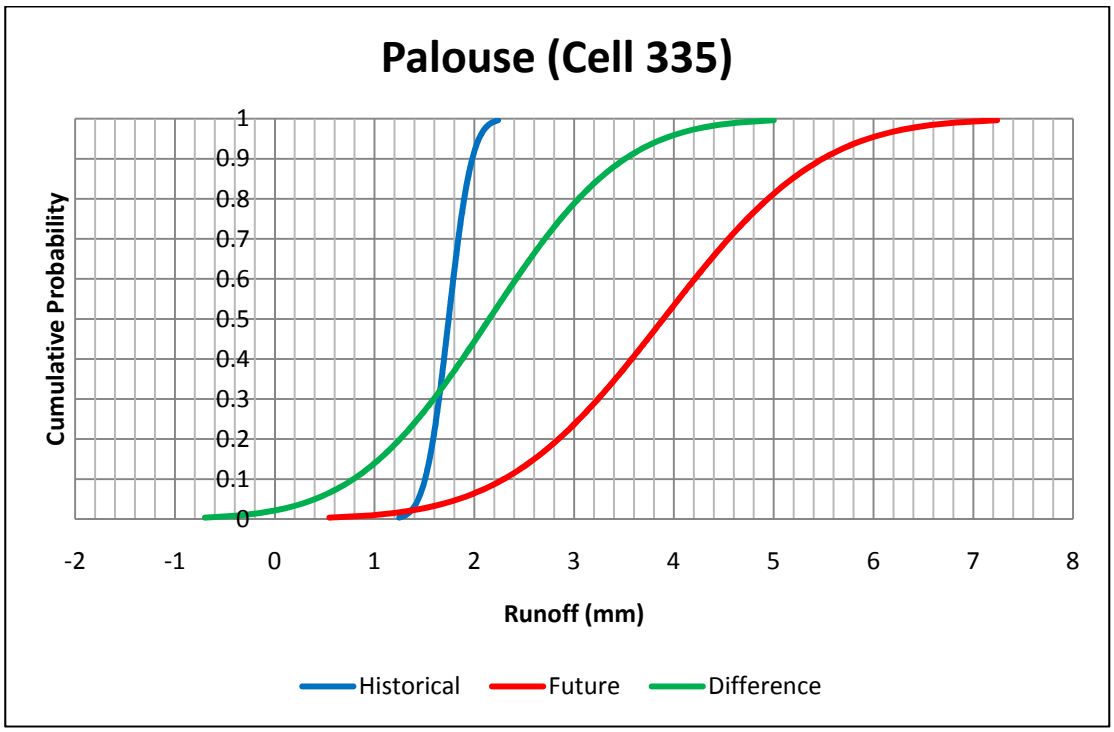

Figure 20: Historical, future and difference 50-year storm runoff CDFs for the grid cell over the Palouse River basin

3.5 Factors Contributing to Forecasting Uncertainty

For the four factors that were controlled in order to assess the uncertainty in assessing future runoff regimes, each was isolated in terms of its individual effect while averaging the remaining components based on their selection in the Monte Carlo simulation. For the analysis of each component, the sample space for that component contained all of the random selections of the four parameters that contained that component. This creates results that reflect the weighting scheme for the remaining three parameters, but ignores the component being analyzed, so that its individual effect can be interpreted.

3.5.1 Choice of Greenhouse Gas Emissions Scenario

The two emissions scenarios, A1B and B1, were selected to be the "worst" and "best" case scenarios for the 2040s climate, respectively. In terms of average response over the domain, the mean and standard deviation for the two scenarios showed a small change as shown in table 6. However, when regarding the spatial distribution of the runoff event, there is notable difference in the two emissions scenarios. The percent change from the historical runoff depth has an entirely different spatial pattern for each of the two scenarios, with regions responding differently to varying amounts of warming. Figure 21 shows the percent change from the historical runoff depth to the Monte Carlo simulated future depth for the A1B and B1 emissions scenarios for the 50-year storm.

Table 6: Monte Carlo simulated mean and standard deviation of runoff for the 425 grid cells of the PNW due to isolation of the A1B and B1 emissions scenarios for the 50-year storm

	A1B	B1
Mean Runoff for PNW (mm)	18.82	18.34
Standard Deviation of Runoff for PNW (mm)	24.86	24.27

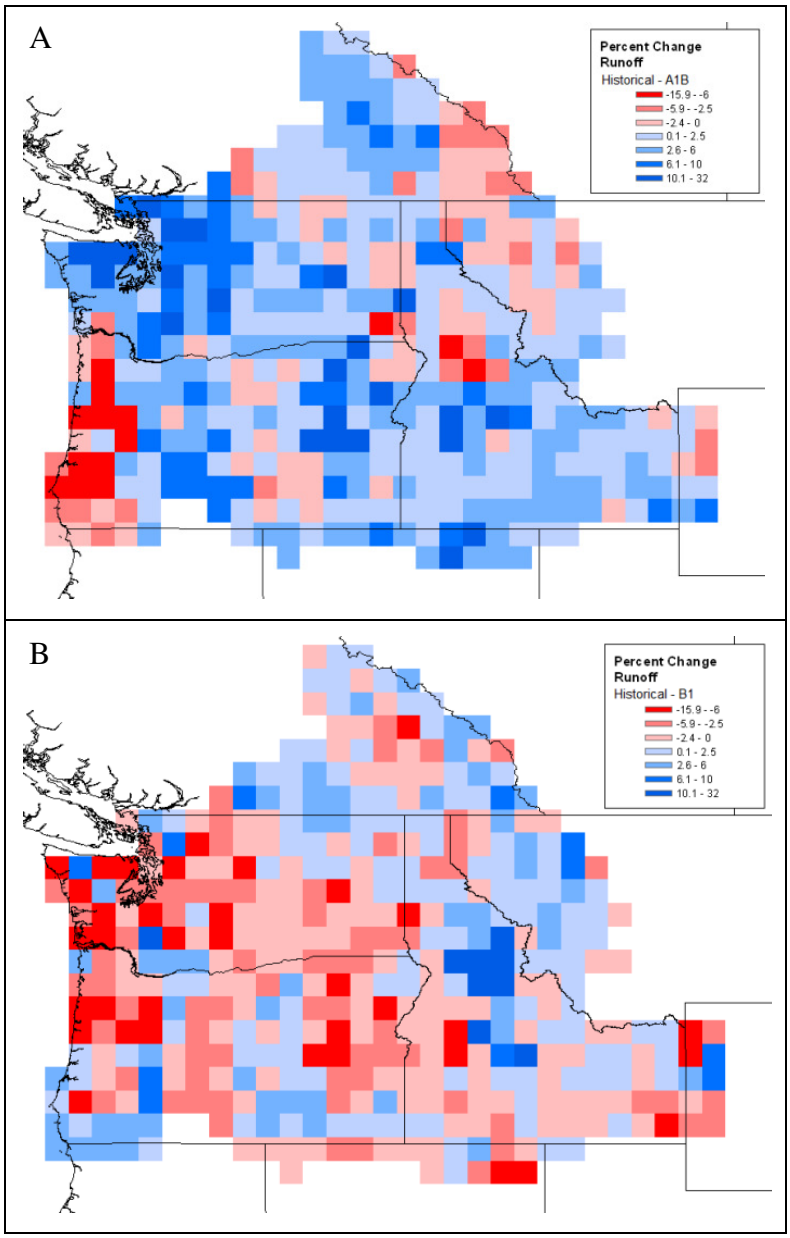

Figure 21: Percent change in runoff for the 50-year storm from the historical climate to A) the A1B emissions scenario and B) the B1 emissions scenario

In figure 22, the difference between the runoff from the A1B and B1 scenarios for the 50-year event is shown over the domain. The average difference in temperature anomaly in the 2040s for the two scenarios as modeled by the suite of GCMs in Mote and Salathé (2010) is around 0.5 ºC, but the difference in precipitation averaged over the PNW is nearly zero. However, more local changes are evident in the difference displayed by figure 21. Most of the domain had decreasing runoff due to the B1 scenario simulations with the largest decreases west of the Cascade Mountains near Puget Sound. However, for the A1B scenario, the Puget Sound region and Olympic Peninsula show the largest increases. Much of the domain shows increases in runoff due to the A1B scenario. It is important to note that these emissions scenarios drive the GCM projections and therefore the snowpack and soil moisture simulations, so the uncertainty due to emissions scenarios is also a part of any further analysis.

Figure 18 shows the difference between the A1B and B1 scenarios in terms of the historical runoff depth. In most of the area around Puget Sound, the higher warming scenario (A1B) increased runoff, and the difference in runoff represents at least 7.5% of the historical runoff depth and as much as 39.8% in the northern Olympic Peninsula around Port Angeles and Sequim, WA. In contrast, the coastal areas of southern Oregon and northern California project less runoff for the A1B scenario nearly 8.8 mm, in some areas representing 8.5% of the historical runoff depth. Central Idaho is projected to have 4.4 mm less runoff due to the A1B emissions scenario compared to B1; however, this represents more than 27.5% of the historical runoff depth at that location.

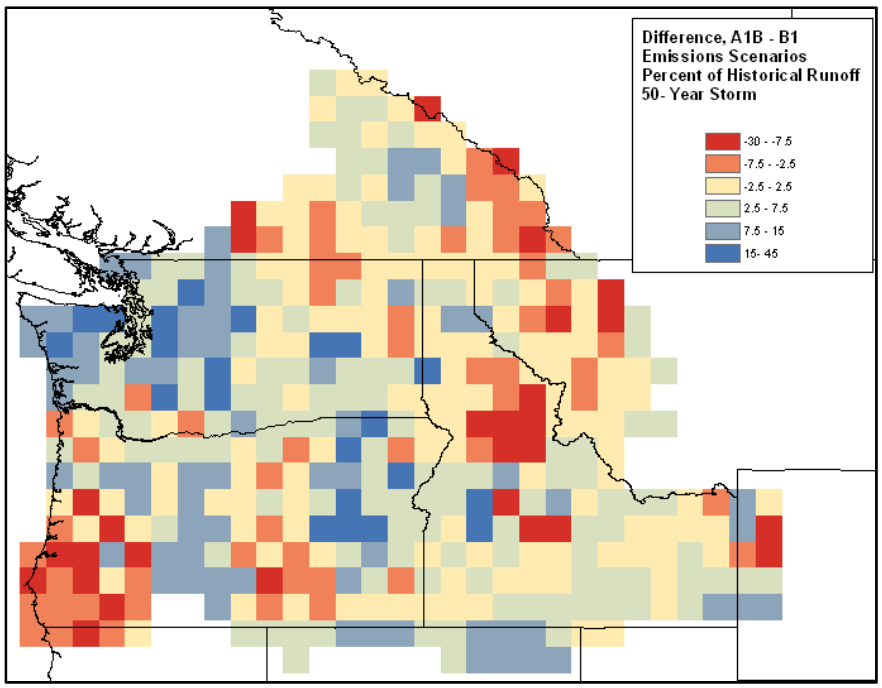

Figure 22: Difference in runoff depths for the 50-year storm due to A1B and B1 emissions scenario as a percent of historical runoff due to the 50-year storm.

3.5.2 Choice of Global Climate Model

The GCMs in this suite were ranked by their relative biases (see table 2) in re-creating the climate over the Pacific Northwest for the years 1970-1999 as determined by Mote and Salathé (2010). After isolating the effect of GCM selection, it was found that a significant factor in determining the projected effect on runoff was the precipitation bias found in the historical hindcasting (the hindcasting was described in section 2.5). Figure 23 shows the relationship between hindcasting precipitation bias for each model and the 425-cell grid mean runoff and the grid standard deviation of runoff for the 50-year storm. The trends were both found significant at 95%. An increased precipitation bias in the models was correlated to an increase in both the mean and the standard deviation of the runoff response in the future scenario.

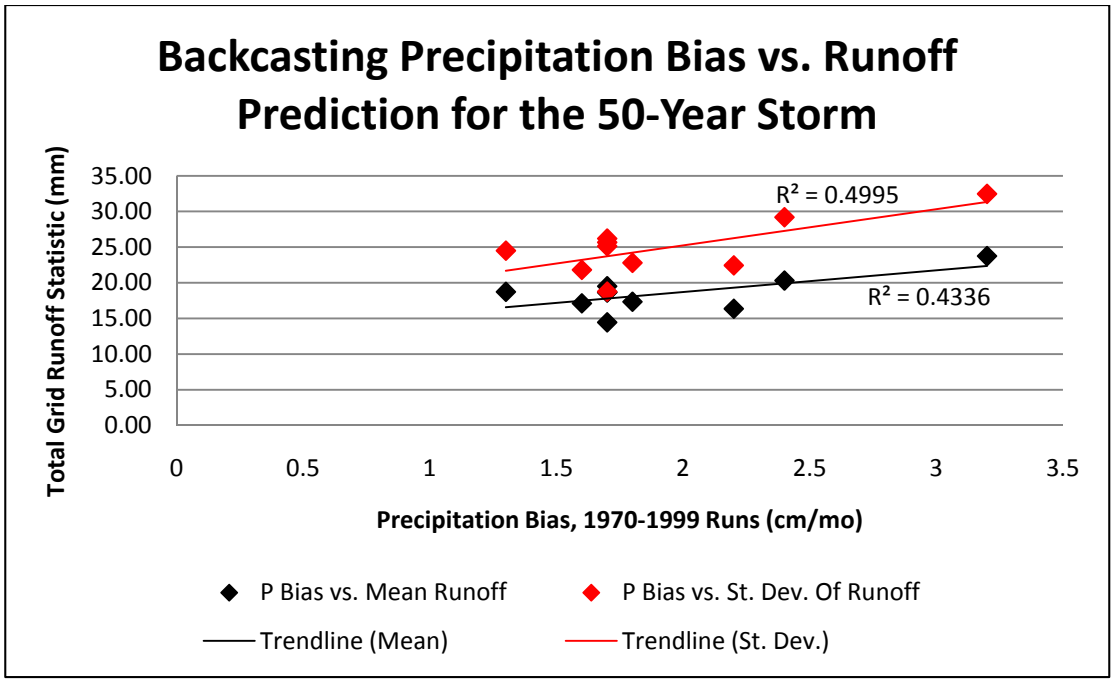

Figure 23: Plot of average precipitation bias for each GCM for hindcasting 1970-1999 climate against 425-cell mean and standard deviation for future 50-year storm. GCM isolated with random sampling of emissions scenario, soil moisture and snow water-equivalent value with line of best fit and coefficient of determination.

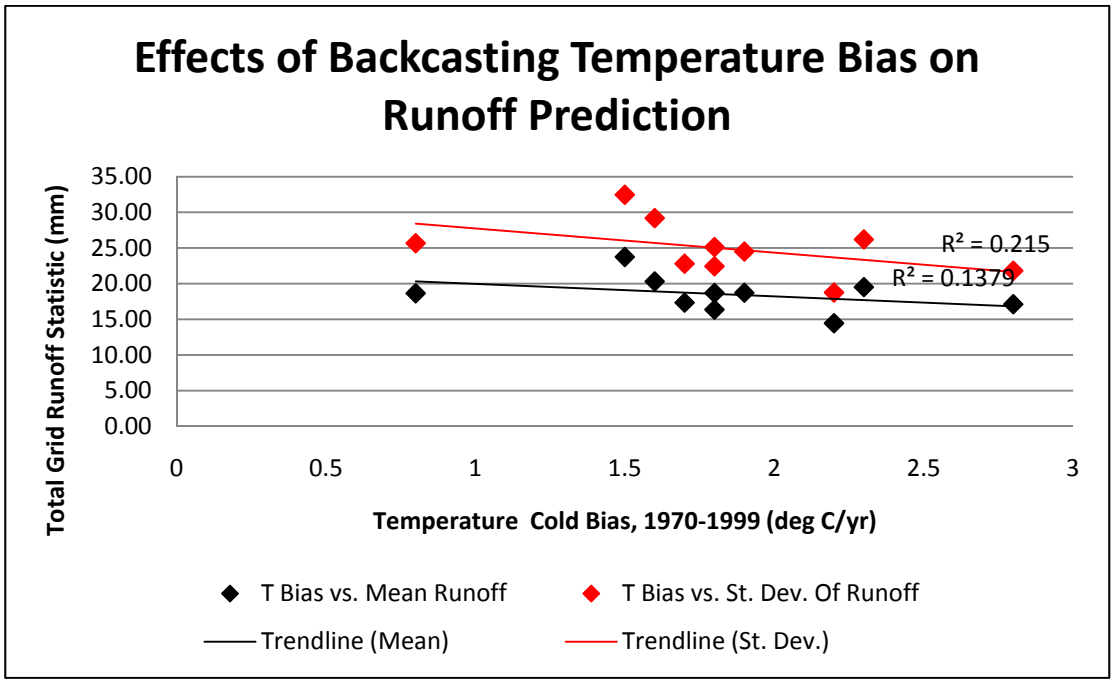

Figure 24: Plot of average temperature cold (negative) bias for each GCM for hindcasting 1970-1999 climate against 425-cell mean and standard deviation for future 50-year storm. GCM isolated with random sampling of emissions scenario, soil moisture and snow water-equivalent value with line of best fit and coefficient of determination.

There also existed trends in the effect of temperature bias on the runoff mean and standard deviation; however, they were not found statistically significant at 95%. The relationships between the temperature bias and the grid runoff parameters are shown in figure 24.

The CNRM CM3 model was found to perform the best in terms of having the smallest overall hindcasting bias, as reported in table 2, and thus it was given the highest probability in the Monte Carlo simulation. CNRM CM3's average T bias was -0.8 °C/yr and its average P bias was 1.7 cm/mo over the PNW. The weighted result of all of the CNRM CM3 runs is shown below in figure 25. In comparison, the HADCM model had the lowest precipitation bias of the ensemble of GCMs, and the weighted results of all runs with the HADCM data are shown in figure 26 below. HADCM's average T bias was -1.9 °C/yr and its average P bias was 1.3 cm/mo. While the spatial distribution of runoff is basically identical, the magnitude of the runoff varies slightly. Although the HADCM model had a lower precipitation bias for the 1970-1999 climate runs, the model had a slightly higher mean runoff and higher variance than would be indicated by its bias as indicated in figure 23 above. However, the cold (negative) bias was larger for HADCM than CNRM CM3, and while the trend for temperature was not statistically significant the T bias could still play a role in the GCM's overall prediction. The variability introduced by the selection of GCMs is illustrated in figure 27 as a plot of the CV for the results isolated by GCM.

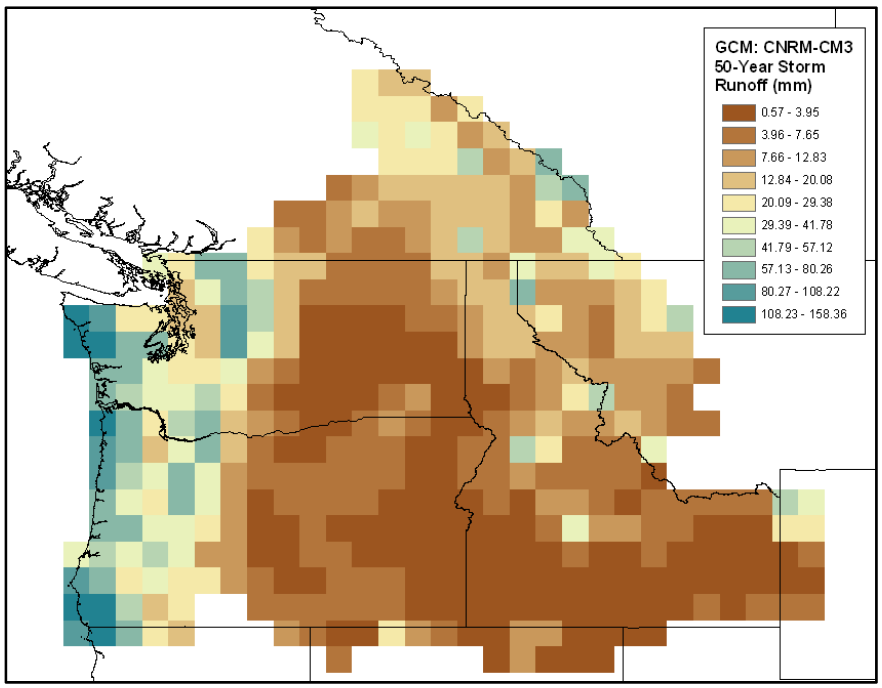

Figure 25: Runoff depth for the future 50-year storm for the model with highest selection probability according to hindcasting bias for 1970-1999 (CNRM CM3) with random selection of emissions scenario, soil moisture and snow water-equivalent. Average T bias = -0.8 °C/yr, average P bias 1.7 cm/mo.

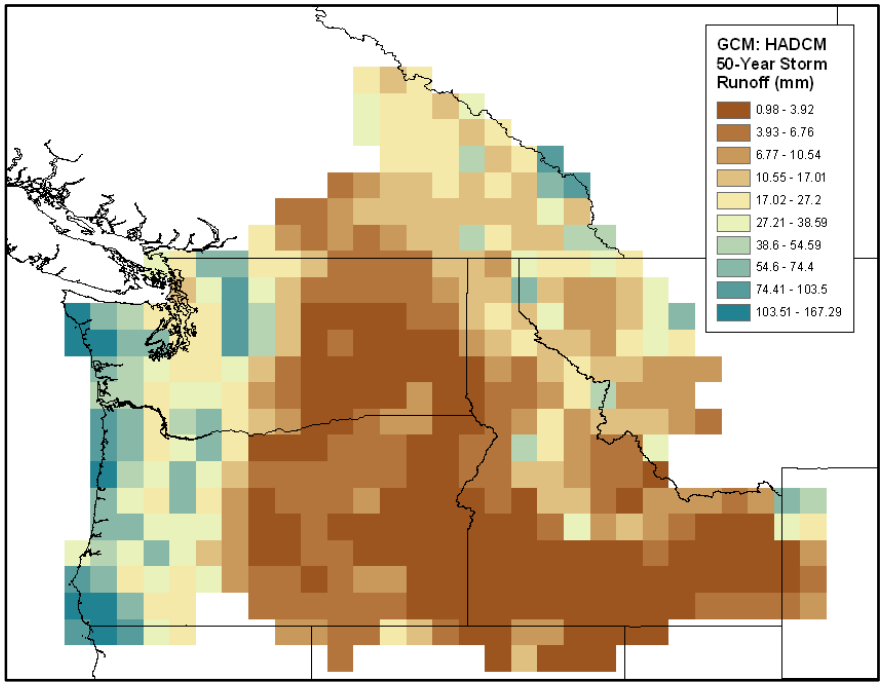

Figure 26: Runoff depth for the future 50-year storm for the lowest precipitation bias model for hindcasting 1970-1999 climate (HADCM) with random selection of emissions scenario, soil moisture and snow water-equivalent. Average T bias = -1.9 °C/yr, average P bias 1.3 cm/mo.

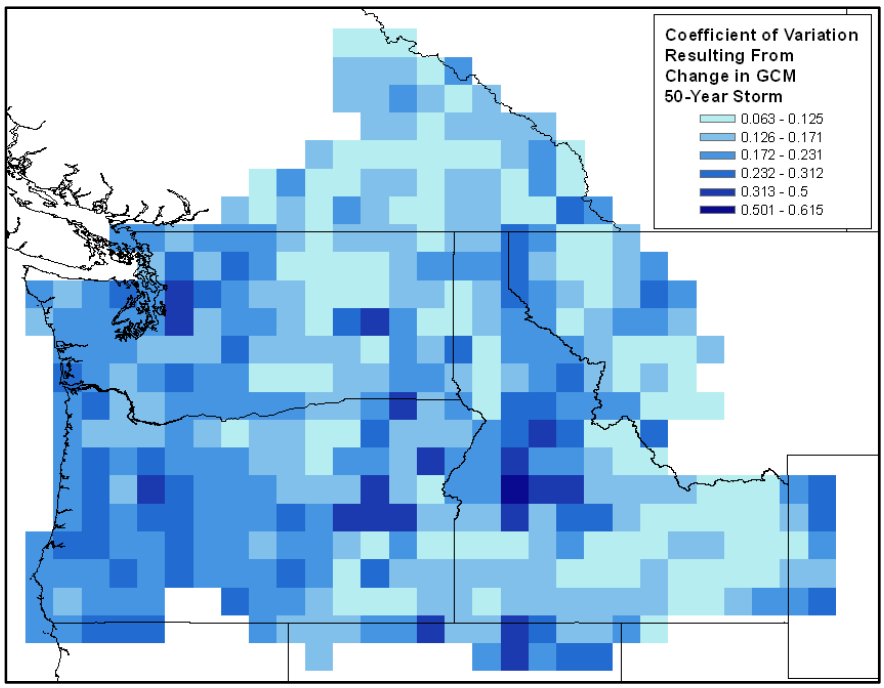

Figure 27: Coefficient of variation for runoff due to the 50-year storm by isolated GCM. The resulting runoff from the Monte Carlo simulation for each GCM is summarized by the CV for the forecasts by each GCM.

3.5.3 Antecedent Snowpack

Because the interactions of snowpack with precipitation can reduce or increase runoff volumes due to either capture of rainfall by snowpack thereby preventing runoff, or by snowmelt, different locations in the domain behave differently with the presence of snowpack. VIC models both the addition of water to snowpack from rainfall and the contribution of snowmelt to runoff. Figure 28 shows the difference between the low snowpack condition (the 12.5% quantile) and the high snowpack condition (87.5%) for the 50-year storm. Because we are analyzing only liquid precipitation events, when temperatures are warmer (see figure 3), the amount of influence from snowpack is likely to be reduced in these events. The areas where rain-on-snow events are more frequent are more likely to show sensitivity in this experiment.

The most notable area for this is generally in and west of the Cascade Mountains, where the peak annual rainfall event tended to be in fall and winter. West of the Cascades and in the mountain range in Washington and Oregon show increases in runoff with a decrease in snowpack, while the Canadian Rockies and south into Montana show decreases in runoff with a reduced snowpack. Most of the Pacific Northwest, including almost the entire region between the Cascades and the Rockies, shows no sensitivity to the change in snowpack and is likely not an important factor during the time of year these storm events were simulated. Table 7 shows the relationship between the mean and standard deviation of the runoff from the 50-year event for the entire domain in relation to the simulated antecedent snowpack quantiles.

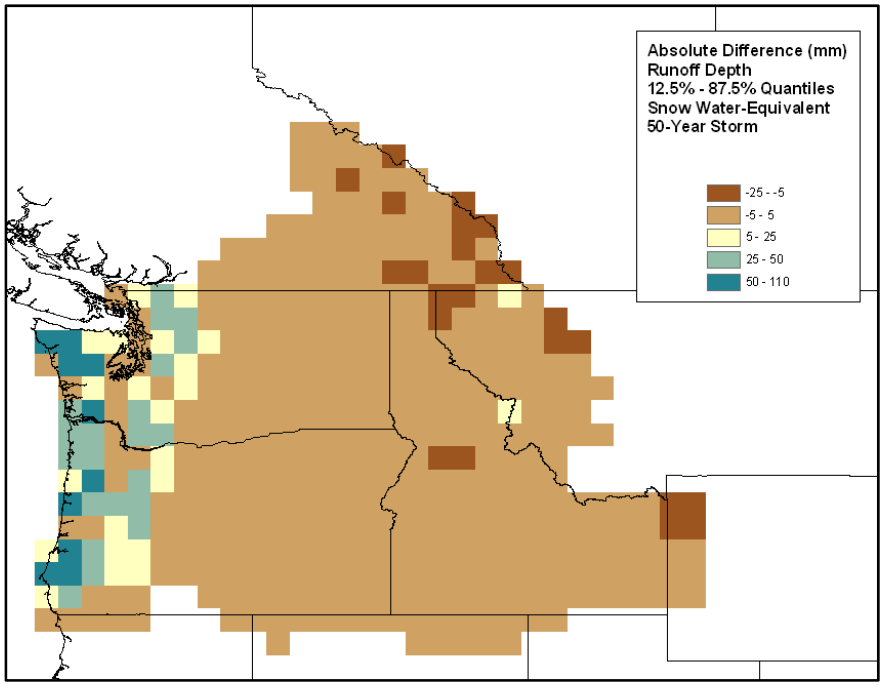

Figure 28: Absolute difference in runoff due to minimum snow water-equivalent (12.5% quantile) and maximum snow water-equivalent (87.5% quantile) for the future 50-year storm with random selection of emissions scenario, GCM and soil moisture

Table 7: Mean and standard deviation of 50-year storm runoff depth for 425 grid cells in the PNW due to snow water-equivalent quantile with random selection of emissions scenario, GCM and soil moisture.

	12.50%	50%	87.50%
Mean Runoff (mm)	20.06	18.74	16.39
Standard Deviation of Runoff (mm)	28.65	25.47	21.32

3.5.4 Antecedent Soil Moisture

The presence of more soil water consistently increased the mean and standard deviation of the runoff depths for the 50-year event, as shown in table 8. While the minimum increase in runoff from the 12.5% soil moisture quantile to the 87.5% quantile was 11.1% of the median soil moisture runoff value, some locations were simulated to have a nearly 250% increase in runoff relative to the median soil moisture runoff. Figure 29 shows the difference in runoff for the 87.5% and 12.5% soil moisture quantiles, in terms of the percent of the median soil moisture runoff value. The locations experiencing the proportionally highest increase in runoff due to an increase in soil moisture were locations at higher elevations in central Idaho, where 50-year storm runoff values were typically 10 to 20 mm.

Table 8: Mean and standard deviation of 50-year storm runoff depth for 425 grid cells in the PNW due to soil moisture quantile with random selection of emissions scenario, GCM and snow water-equivalent.

	12.50%	50%	87.50%
Mean Runoff (mm)	14.70	18.25	22.73
Standard Deviation of Runoff (mm)	20.15	24.54	29.38

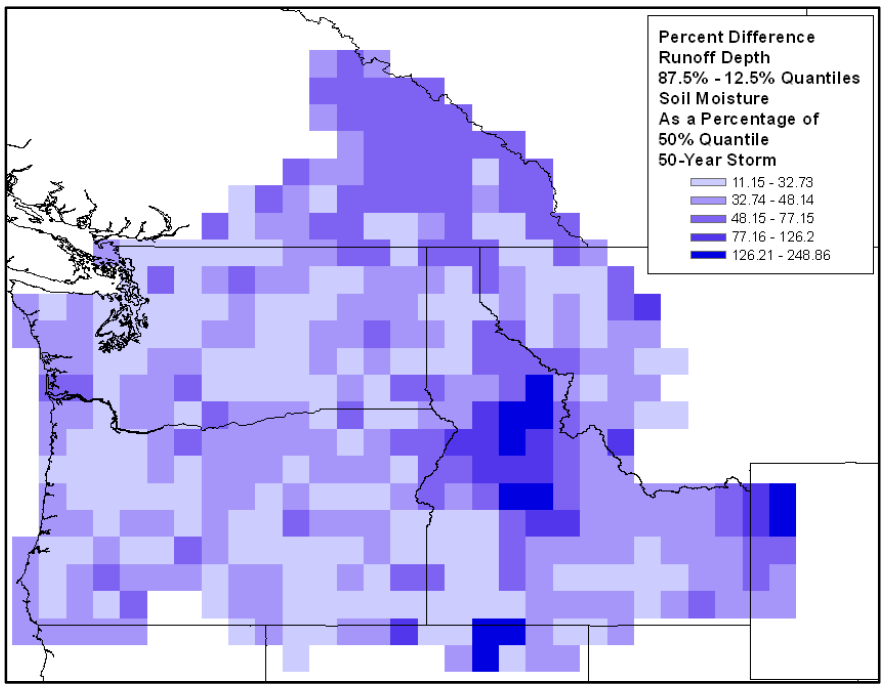

Figure 29: Absolute difference in runoff due to maximum soil moisture (87.5% quantile) and minimum soil moisture (12.5% quantile) for the future 50-year storm with random selection of emissions scenario, GCM and snow water-equivalent

4. Discussion

The combination of several uncertain parameters in estimating future runoff when doing any hydrologic assessment makes it difficult to pin down a single answer as being "correct" when forecasting future hydrologic fluxes such as runoff. While two emissions scenarios were selected in this study, and were intended to reflect the worst and best cases for greenhouse gas emissions in the 2040s, there are infinitely more paths that humans on Earth can follow going forward (Nakićenović and Swart 2000). CO_2 emissions in the early 20th century have already exceeded even the most fossil fuel-intensive emissions scenario (A1FI) developed in the late 1990s by the IPCC (Raupach et al. 2007). This means that the uncertainty in emissions scenario reflected in this study is not all-inclusive, because the actual emissions exceed even the study's "worst case". Because these emissions scenarios drive the GCMs used for creating the future

climate data used to make hydrologic predictions, the uncertainty in their estimates are amplified as other layers of uncertainty are added.

In the case of the runoff analysis, the difference between the worst-case A1B and best-case B1 emissions scenarios was a range of -30% to +45% of the historical runoff, with a strong regional signal. The overall change in mean and variance for the Pacific Northwest was small likely due to temperature-driven increases in evapotranspiration (ET) and decreases in soil moisture counteracting intensified storm events in many places. Because a choice of emissions scenario for modeling has a long-reaching impact on other variables, such as soil moisture and snowpack in this study, the safest approach seems to be a bracketing method to choosing an emissions scenario. By selecting scenarios to model that represent the worst and best case; the risks can be reduced by understanding a basic range of possibility. However in this case, the envelope meant to contain the actual greenhouse gas emissions scenarios was low, and did not bracket the real case.

The selection of GCM in this case offered little insight into understanding changing runoff in the Pacific Northwest. While the magnitude of runoff depth changed slightly between the models, no major changes in the regional signature of the runoff occurred. Also, as shown in figure 19, the results from a particular GCM are strongly correlated to the precipitation bias of the GCM when evaluating past climate conditions. Thus, evaluations such as those performed by Mote and Salathé (2010), which ranked the models in terms of their ability to re-create historical climate specifically in the Pacific Northwest, are important for selecting a model that is most “realistic” when performing studies on a particular area. Different GCMs have different

strengths and weaknesses, and will perform better over different regions based on parameterization and assumptions made for solving planetary atmospheric and oceanic circulation within the model. Selecting model output that best describes the region of interest is important for performing experiments for future climate in that region. While the hindcasting ability of a GCM does not necessarily evaluate the ability of a model to predict changes in the climate going forward, it is clear that the future scenarios that are forecasted reflect the bias that each model has when evaluating the historical climate.

Soil moisture and snowpack conditions in the future are affected by a warming climate. Increased temperatures cause an increase in soil moisture loss to evapotranspiration and a reduction in water stored as snowpack, which were shown in figure 10. These effects can change the amount, and especially in the case of snowpack, the timing of runoff. Because snowpack storage declines in a warmer climate, due to earlier melting and a decrease in the amount of precipitation that falls as snow, the effect of spring snowmelt-caused runoff decreases. Figure 28 demonstrates that decreased snowpack is correlated to increasing runoff in many places in the Pacific Northwest. While this study did not specifically examine the effects of climate change on winter runoff events, many of the events were “staged” to take place in winter conditions (figure 3). In the locations where snowpack had significant presence when the annual maximum events occurred most frequently, such as the Olympic Peninsula, the decreased presence of snowpack was related to a large (greater than 50%) increase in runoff due to the 50-year event in the future, as in figure 28.

While a minimum change of +11% of the median soil moisture runoff depth was observed for the difference between the highest and lowest quantiles, there was no clear trend in where the soil moisture effects would be greatest. Predicting soil moisture in a changing climate would prove difficult because of the estimate of the water balance of the soil layers. Precipitation is the greatest predictor for soil moisture, and precipitation changes in the future are highly uncertain according to emissions scenario and GCM.

The areas at highest risk due to changes in runoff are the locations that in general already receive a large amount of runoff and which are projected to experience a large average increase in runoff for common design events. One such area is the Olympic Peninsula, which experiences the heaviest precipitation in the Pacific Northwest and produces the highest runoff, but is also projected by weighted average to increase runoff production, in some cases by more than 10% (refer to figures 11, 12 and 13). However, as shown in figure 16, this area is also the most uncertain in terms of the range of events simulated using this method. While the prediction is fraught with uncertainty, the consensus of the models in the suite show that runoff due to these common design storm events in the Pacific Northwest will increase.

Although in this study, we quantified the uncertainty associated with the various inputs to a hydrologic assessment, we are not exhaustive in that effort. One component contributing to forecasting uncertainty that went unanalyzed in this study is that of the methodology used for downscaling the meteorological data. While the emissions scenarios and GCMs project different versions of a future climate, no clear pattern in change related to the topography and characteristic weather of the PNW emerges on a broad scale. The coarse 1/2 degree resolution

for the hydrologic simulation also contributes to this uncertainty, as it averages a large number of explicit features that would characterize changes. In the case of emissions scenarios, the pattern created in the difference between the A1B and B1 runs (figures 21 and 22) tells us little about what different warming scenarios will do in the Pacific Northwest because there is no clear correlation between amount of warming and changes in runoff. Some locations that were simulated to decrease in runoff under a B1 scenario showed large increases in the A1B scenario, so extrapolating that trend is difficult to a warming scenario above the A1B levels. Pinning down the cause of this is more difficult, but spatial issues, between downscaling large GCM grid cells and 1/2 degree hydrologic simulation, certainly play a role. When downscaling GCM outputs, which often have grid cells between 1 and 5 degrees in latitude and longitude, it is important to capture the regional information contained within that grid cell, especially when estimating extreme events or locations with complicated topography. Salathé et al. (2010) showed that regional climate models to resolve the coarse-resolution GCM outputs to a finer grid, while regarding the complicated topography and coastlines, do a better job of matching regional signatures of meteorology in an area. The "hybrid delta" downscaling method used for the data in this study is limited by historical data and scaling the temperature and precipitation based on GCM-projected changes. However, use of a numerical weather model such as WRF (Michalakes et al. 1998) or a regional climate model (RCM) similar to Salathé et al (2010) could produce dynamically-downscaled meteorology data for a future climate which could represent the changes in climate on a finer temporal scale, as well as resolving explicitly important regional features, such as changes in elevation, on a finer spatial scale.

4.1 Limitations

There were three major limitations resulting in systematic low biases within this study. The first was the use of the daily timestep. Because the meteorological data were at a 24-hour timestep by calendar day, a systematic low bias was introduced for the 24-hour events. Instead of considering the annual maximum 24-hour precipitation totals, which could span two days, the largest calendar day total was considered instead. Another limitation was the aggregation and spatial scale for the hydrologic model. Because the parameters and meteorological data were aggregated from 1/16 to 1/2 degree, the most extreme features were averaged out with each step of aggregation. This is significant when addressing grid cells that experience the most extreme precipitation, as the coarser resolution cell would not reflect the intensity of the most intense fine resolution event contained within it. In places with large changes in elevation and therefore precipitation, such as the Olympic Peninsula or the Cascade Mountains, cells with very high precipitation and a high risk regarding runoff may be averaged with several low-intensity cells, reducing the visible risk in that area. The third major limitation arises from the VIC model itself. VIC is capable of simulating the effects of frozen soils, which could have a significant impact on runoff in areas where rainfall occurs in times when the water content of the soil is frozen. This creates a systematic low bias in the results for runoff.

For selecting GCMs, the probability of selection was based equally on the hindcasting temperature and precipitation biases. While the importance of precipitation relative to temperature in creating runoff is spatially variable, it is difficult to quantify the importance of each in evaluating which model is “better” at predicting the future climate. Thus, the weight for

temperature bias and precipitation bias were considered equally. In locations with a dry climate and high temperatures, the effects of ET induced by temperature may be significant, and in wetter climates the precipitation inputs may dominate the runoff regime. Thus there was no scientific way to assign a weight to the bias for the temperature and precipitation.

When selecting the quantiles for SWE and soil moisture, it was assumed that the two were fully independent in their selection. While for most grid cells in the domain the values for SWE and soil moisture were independent, there are other cells where the correlation between the two parameters is significant. In the cases where this is true, the correlation of the values would lead to less uncertainty about their estimates, as the values for each that occur are dependent.

A significant limitation occurs for the design of water control structures in eastern Washington, where the heaviest rainfall often does not lead to the most runoff. While structures are designed to handle runoff due to a storm with some return interval, the most significant runoff events are due to snowmelt contributions and do not typically occur when rainfall is heaviest. For the drier part of the year, soil moisture is low and any rainfall will be infiltrated quickly, but during the wet part of the year, the increased soil moisture and snowmelt input to runoff can increase the runoff depth even with lower precipitation events. As mentioned before, this is the same as saying that the 50-year storm does not always cause the 50-year flood. In these cases less intense storms can lead to intense runoff simply by the peripheral conditions.

The 14-day window used for averaging climate to produce synthetic meteorological data was not changed in time for the future cases, which may not capture the changing seasonality of

precipitation and the changing temperatures and wind speeds associated with a different season or even the difference in 14-day periods.

A significant factor to snowmelt is the increased wind speed associated with storms. This can be more important to melting snow than the advection of heat due to rainfall and may not be adequately captured by the synthetic meteorological data for the storm events. This can lead to an underestimation of snowmelt to runoff in places with high SWE during the time of the annual maximum event.

4.2 Future Directions of Study

In this study we only evaluated the effects of one downscaling method. As extensively discussed previously, the comparison of a dynamic downscaling method to the delta method could produce interesting results regarding the effects of the Pacific Northwest's complicated topography. Investigating changing contributions of snowmelt and snowpack to runoff in a warming climate would offer insight into areas where runoff makes a significant contribution to runoff and streamflow, specifically west of the Cascades. Running VIC at a finer resolution, such as 1/8 or 1/16 degree, could resolve specific local instances of changing runoff that would make the result of these effects more relevant at a local level, such as for implications for stormwater management.

The Pacific Northwest is a very large domain, and the seasonal response of runoff throughout the domain is not homogeneous. There is a distinct regional response within the PNW to runoff

by season, and investigating how runoff behaves for each season due to a seasonal maximum event and including improved estimates for snowpack and soil moisture would improve estimates for runoff. If snowpack and soil moisture were simulated or taken from actual observations for a period leading up to the occurrence of the annual (or seasonal) maximum event, a better estimate for these values in the model that are correlated to some peak event would be employed, thereby improving the runoff estimate further. Additionally, the ability for VIC to capture rain-on-snow events should be assessed, as these events can produce extreme runoff that may not be reflective of the return interval of the precipitation event. In general the investigation of the effects of changing snowpack on runoff would improve estimates for runoff in a changing climate.

5. Conclusions

Using Monte Carlo simulation with the VIC hydrology model, we forecasted runoff conditions in the Pacific Northwest, and this forecast allowed us to answer two questions about the effects of climate change on runoff. First, how will climate change in the Pacific Northwest affect the amount of runoff generated by design storms of common return intervals, comparing historical climate to GCM-simulated future climate, and second, how much uncertainty in projecting runoff in the future is caused by selection of greenhouse gas emissions scenarios, GCMs, and hydrologic modeling of snowpack and soil moisture for future climate scenarios?

The forecast shows a general increase in runoff depth for events caused by design storms of 2, 25, 50 and 100-year average return intervals; however, the uncertainty in this forecast is large.

A majority of locations in the Pacific Northwest show an increase in runoff depth for all of the return intervals tested. While this generally explains why engineers and planners who deal with water have reason to be concerned in the future about runoff, this conclusion alone does not offer any assistance in planning for climate change. While there are tools that exist to attempt to understand the state of the climate going forward, such as the IPCC emissions scenarios and GCM projections for the climate, the range of uncertainty in these tools makes it difficult to precisely quantify changes in measurable hydrologic fluxes, such as runoff. Understanding the source of uncertainty can help avoid making mistakes such as reliance on the output of a single GCM, or even a range of emissions scenarios, which we have discovered are all low (Raupach et al. 2007).

The GCMs and emissions scenarios are the driving factors behind understanding the potential future climate. The range in results for future temperature and precipitation is due to uncertainty from predicting the course of greenhouse gas emissions and the ability of GCMs to produce accurate forecasts of climate in the future in response to the greenhouse gas emissions scenarios. While there is no current way to evaluate the ability of a GCM to produce realistic climate forecasts, the current method of evaluating GCMs by their ability to re-create past climate reveals that a model's bias in this hindcasting is significantly correlated to the results that it will produce in the future. Because all models in this study display a positive "wet" bias for precipitation in hindcasting, some of the resulting projected increases could be due to this effect.

The effect of changing snowpack and soil moisture shows a clear relationship for runoff, with increased soil moisture increasing runoff for all cells in the domain, and reduced snowpack increasing runoff for a majority of the Pacific Northwest. While trends regarding soil moisture and other hydrologic fluxes and states in the face of climate change are not clear due to uncertainties in forecasting precipitation, the reduction in snowpack caused by a warming climate looks to be another mechanism for increasing risk in regard to runoff in the future.

The areas in the Pacific Northwest that are most at risk are the wet regions that historically produce significant runoff and are projected to experience an increase in runoff due to climate change. Thus, parts of the Olympic Peninsula and the Puget Sound region appear to be most at-risk in the future in regard to handling runoff. However, these areas also have the most uncertainty when projecting future runoff depths. The envelope of possible future conditions due to climate change is very large, and due to the uncertainties for each component of making a forecast, achieving high confidence in the probability that a water control structure will not fail in its lifetime of service is much more difficult.

In order to reduce uncertainties in projecting the effects of climate change on runoff in the Pacific Northwest, several steps can be taken toward improving the forecast. The use of dynamically-downscaled climate data would do a better job of characterizing the precipitation regimes encountered in the Pacific Northwest due to complex topography and coastlines, which are not well-characterized by coarse-scale GCM output and the delta downscaling method. The dynamic downscaling may also do a better job of capturing the intensification of precipitation events that is expected to occur due to climate change, and would affect design storms used for

runoff-related design the most. The use of a finer spatial scale for the downscaled results and the hydrologic simulation would do a better job of characterizing extremes as well as local hydrologic response to those extreme events than larger, lumped average cells. Finally, using continuous distributions for the soil moisture and snowpack and a larger sample size for the Monte Carlo simulation of future results would produce a better estimate of the posterior distribution of runoff depths for the future climate scenarios.

Going forward into an uncertain future, this study serves one primary purpose. This study serves as a framework for engineers and planners who need to plan for risks associated with climate change in the future. Many current practices rely on a single emissions scenario and GCM forecast to make a forecast for future conditions. This study has shown that the individual selection of either of these parameters to achieve a result runs the risk of being misleading, because the variability in result that occurs from the selection of either parameter is very high. By considering a range of possibilities and evaluating the central tendency in the results for climate change projections, an appropriate amount of risk can be assumed. A single point gives no assurance of reliability whatsoever. This is also a warning to those in areas sensitive to flooding or to runoff-related problems such as erosion. While the historical 25-year event is expected to be exceeded in only 4% of years in a stationary climate, the increased intensity of these extreme events in a changing climate means the storm or flood with the intensity equal to the historical 25-year event will be exceeded more often. This holds for events of all average return intervals – the intensity of an event associated with a long ARI would increase, and the ARI for that specific intensity would decrease.

6. References

Bedient, P. B., W. C. Huber, and B. E. Vieux (2008), *Hydrology and Floodplain Analysis*, 4 ed., 795 pp., Prentice-Hall, Inc., Upper Saddle River, NJ 07458.

Cane, M., S. Zebiak, and S. Dolan (1986), Experimental forecasts of El-Nino, *Nature*, *321*, 827-832.

Cashwell, E. D., C. J. Everett, and Los Alamos Scientific Laboratory. (1959), *A Practical Manual on the Monte Carlo Method for Random Walk Problems*, 153 pp., Pergamon Press, New York,.

Castillo, V. M., A. Gómez-Plaza, and M. Martínez-Mena (2003), The role of antecedent soil water content in the runoff response of semiarid catchments: a simulation approach, *Journal of Hydrology*, *284(1)*, 114-130.

Cherkauer, K., and D. Lettenmaier (1999), Hydrologic effects of frozen soils in the upper Mississippi River basin, *Journal of Geophysical Research-Atmospheres*, *104(D16)*, 19599-19610.

Chow, V. T., D. R. Maidment, and L. W. Mays, (1988), *Applied Hydrology*, 572 pp., McGraw-Hill, New York.

Dingman, S. L. (2002), *Physical Hydrology*, 2nd ed., 600 pp., Prentice Hall.

Dupuis, D., and M. Tsao (1998), A hybrid estimator for generalized Pareto and extreme-value distributions, *Communications in Statistics-Theory and Methods*, *27(4)*, 925-941.

Elsner, M., L. Cuo, N. Voisin, J. Deems, A. Hamlet, J. Vano, K. Mickelson, S. Lee, and D. Lettenmaier (2010), Implications of 21st century climate change for the hydrology of Washington State, *Climatic Change*, *102*, *225*-260.

FAO (1998), Digital soil map of the world and derived soil properties, *Land and Water Digital Media Series*.

Frei, C., C. Schar, D. Luthi, and H. Davies (1998), Heavy precipitation processes in a warmer climate, *Geophysical Research Letters*, *25(9)*, 1431-1434.

Gao, H., Q. Tang, X. Shi, C. Zhu, T. J. Bohn, F. Su, J. Sheffield, M. Pan, D. P. Lettenmaier, and E. F. Wood (2010), Water Budget Record from Variable Infiltration Capacity (VIC) Model, *Algorithm Theoretical Basis Document for Terrestrial Water Cycle Data Records*, (In Review).

Gilchrist, W. (2000), *Statistical Modelling with Quantile Functions*, 344 pp., Chapman and Hall/CRC.

Giorgi, F., and L. Mearns (2003), Probability of regional climate change based on the Reliability Ensemble Averaging (REA) method, *Geophysical Research Letters*, *30*, 1629-1632.

Hamlet, A., and D. Lettenmaier (1999), Effects of climate change on hydrology and water resources in the Columbia River basin, *Journal of the American Water Resources Association*, *35(6)*, 1597-1623.

Hamlet, A., and D. Lettenmaier (2005), Production of temporally consistent gridded precipitation and temperature fields for the continental United States, *Journal of Hydrometeorology*, *6*, 330-336.

Hansen, M. C., R. S. DeFries, J. R. G. Townshend, and R. Sohlberg (2000), Global land cover classification at 1 km spatial resolution using a classification tree approach, *International Journal of Remote Sensing*, *21*, 1331-1364.

Hosking, J. (1992), Moments or L-moments - an example comparing 2 measures of distributional shape, *American Statistician*, *46(3)*, 186-189.

Hosking, J. R. M., and J. R. Wallis (1997), *Regional Frequency Analysis: An Approach Based On L-Moments*, Cambridge University Press.

Kalnay, E., et al. (1996), The NCEP/NCAR 40-year reanalysis project, *Bulletin of the American Meteorological Society*, *21*, 437-471.

Kharin, V., and F. Zwiers (2000), Changes in the extremes in an ensemble of transient climate simulations with a coupled atmosphere-ocean GCM, *Journal of Climate*, *13*, 3760-3788.

Kleidorfer, M., M. Moderl, R. Sitzenfrei, C. Urich, and W. Rauch (2009), A case independent approach on the impact of climate change effects on combined sewer system performance, *Water Science and Technology*, *60.6*, 1555-1564.

Labib, F., and E. O'Brien (2005), 2005 Stormwater Management Manual for Western Washington: Volume III - Hydrologic Analysis and Flow Control Design/BMPs *Rep.*, State of Washington Department of Ecology.

Liang, X., D. Lettenmaier, E Wood, and S. Burges (1994), A simple hydrologically based model of land-surface water and energy fluxes for general-circulation models, *Journal of Geophysical Research-Atmospheres*, *99(D7)*, 14415-14428.

Linsley, R. (1986), Flood estimates - How good are they, *Water Resources Research*, *22(9S)*, S159-S164.

Lohmann, D., R. Nolte-Holube, and E. Raschke (1996), A large-scale horizontal routing model to be coupled to land surface parametrization schemes, *Tellus Series a-Dynamic Meteorology and Oceanography*, 708-721.

Loukas, A. (2002), Flood frequency estimation by a derived distribution procedure, *Journal of Hydrology*, *255*, 69-89.

Loukas, A., and M. Quick (1996), Spatial and temporal distribution of storm precipitation in southwestern British Columbia, *Journal of Hydrology*, *174*, 37-56.

Mannshardt-Shamseldin, E. C., R. L. Smith, S. R. Sain, L. O. Mearns, and D. Cooley (2010), Downscaling Extremes: A Comparison of Extreme Value Distributions in Point-Source and Gridded Precipitation Data, *The Annals of Applied Statistics*, *4*(1), 484-502.

Mantua, N., and S. Hare (2002), The Pacific decadal oscillation, *Journal of Oceanography*, *58(1)*, 35-44.

Marks, D., J. Kimball, D. Tingey, and T. Link (1998), The sensitivity of snowmelt processes to climate conditions and forest cover during rain-on-snow: a case study of the 1996 Pacific Northwest flood, *Hydrological Processes*, *12(10-11)*, 1569-1587.

Marks, D., T. Link, A. Winstral, and D. Garen (2001), Simulating snowmelt processes during rain-on-snow over a semi-arid mountain basin, *Annals of Glaciology, 32, 2001*, 195-202.

Marshall, L., D. Nott, and A. Sharma (2004), A comparative study of Markov chain Monte Carlo methods for conceptual rainfall-runoff modeling, *Water Resources Research*, *40*.

Matsumoto, M., and T. Nishimura (1998), Mersenne Twister: A 623-Dimensionally Equidistributed Uniform Pseudo-Random Number Generator, *ACM Transactions on Modeling and Computer Simulation*, *8(1)*, 3-30.

Maurer, E., A. Wood, J. Adam, D. Lettenmaier, and B. Nijssen (2002), A long-term hydrologically based dataset of land surface fluxes and states for the conterminous United States, *Journal of Climate*, *15*, 3237-3251.

Metropolis, N., and S. Ulam (1949), The Monte Carlo Method, *Journal of the American Statistical Association*, *44(247)*, 335-341.

Michalakes, J., J. Dudhia, D. Gill, J. Klemp, and W. Skamarock (1998), Design of a next-generation regional weather research and forecast model, paper presented at Towards Teracomputing, World Scientific, River Edge, New Jersey.

Miller, D. A., and R. A. White (1998), A conterminous United States multilayer soil characteristcs dataset for regional climate and hydrology modeling, *Earth Interactions*.

Milly, P., J. Betancourt, M. Falkenmark, R. Hirsch, Z. Kundzewicz, D. Lettenmaier, and R. Stouffer (2008), Climate change - Stationarity is dead: Whither water management?, *Science*, *319*, 573-574.

Mitchell, T., T. Carter, P. Jones, M. Hulme, and M. New (2004), A comprehensive set of climate scenarios for Europe and the globe: the observed record (1901–2000) and 16 scenarios (2001–2100) *Rep.*, Tyndall Centre Working Paper No 55, University of East Anglia, Norwich, UK.

Mote, P., and E. Salathe (2010), Future climate in the Pacific Northwest, *Climatic Change*, *102*, 29-50.

Nakićenović, N., and R. Swart (eds.), (2000), Special Report on Emissions Scenarios. A Special Report of Working Group III of the Intergovernmental Panel on Climate Change. Cambridge University Press, Cambridge, United Kingdom and New York, NY, USA, 599.

New, M., and M. Hulme (2000), Representing uncertainty in climate change scenarios: a Monte-Carlo approach, *Integrated Assessment*, *1*, 203-213.

NRCS (1986), TR-55: Urban Hydrology for Small Watersheds.

Rahman, A., P. Weinmann, T. Hoang, and E. Laurenson (2002), Monte Carlo simulation of flood frequency curves from rainfall, *Journal of Hydrology*, *256*, 196-210.

Raupach, M., G. Marland, P. Ciais, C. Le Quere, J. Canadell, G. Klepper, and C. Field (2007), Global and regional drivers of accelerating CO2 emissions, *Proceedings of the National Academy of Sciences of the United States of America*, 10288-10293.

Rosenberg, E., P. Keys, D. Booth, D. Hartley, J. Burkey, A. Steinemann, and D. Lettenmaier (2010), Precipitation extremes and the impacts of climate change on stormwater infrastructure in Washington State, *Climatic Change*, *102*, 319-349.

Rubinstein, R. Y. (1981), *Simulation and the Monte Carlo method*, 278 pp., Wiley, New York.

Salathe, E., L. Leung, Y. Qian, and Y. Zhang (2010), Regional climate model projections for the State of Washington, *Climatic Change*, *102*, 51-75.

Sobol, I. M. (1974), *The Monte Carlo method*, 64 pp., University of Chicago Press, Chicago.

Stedinger, J. (2000), Flood Frequency Analysis and Statistical Simulation of Flood Risk, in *Inland Flood Hazards: Human, Riparian and Aquatic Communities*, edited by E. E. Wohl, p. 498, Cambridge University Press.

Tasker, G. (1983), Effective record length for the T-year event, *Journal of Hydrology*, 64, 39-47.

Voutier, P. M. (2010), A New Approximation to the Normal Distribution Quantile Function, edited, Cornell University.

Wallis, J. R., N. Matalas, and J. R. Slack (1974), Just a moment!, *Water Resources Research*, *10*(2), 211-219.

Waring, R. H., and J. F. Franklin (1979), Evergreen coniferous forests of the Pacific Northwest, *Science*, *204*, 1380-1386.

Washington Deparment of Ecology (2004), Stormwater Management Manual for Eastern Washington *Rep.*, 715 pp, State of Washington Department of Ecology.

Wei, L., B. Zhang, M. Wang (2007), Effects of antecedent soil moisture on runoff and soil erosion in alley cropping systems, *Agricultural Water Management*, *94*, 54-62.

Wilby, R., and I. Harris (2006), A framework for assessing uncertainties in climate change impacts: Low-flow scenarios for the River Thames, UK, *Water Resources Research*, *42*.

Zwiers, F., and V. Kharin (1998), Changes in the extremes of the climate simulated by CCC GCM2 under CO2 doubling, *Journal of Climate*, *11*, 2200-2222.

7. Appendix

A.1 24-Hour Design Storm Intensities for the Pacific Northwest

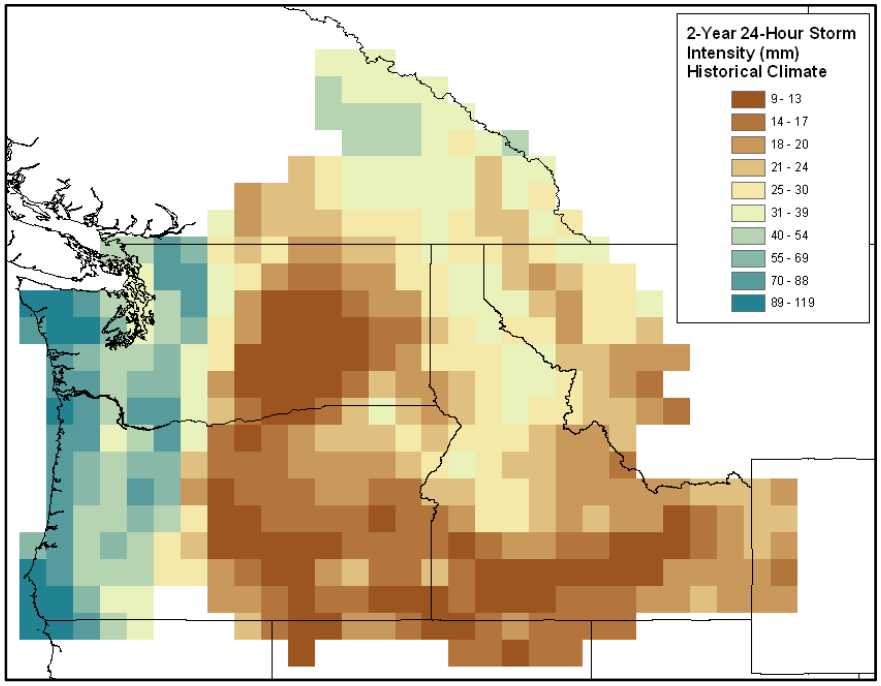

Appendix Figure 1: Historical 2-Year 24-Hour Storm Intensity (mm) as fit to GEV distribution using the method of L-moments

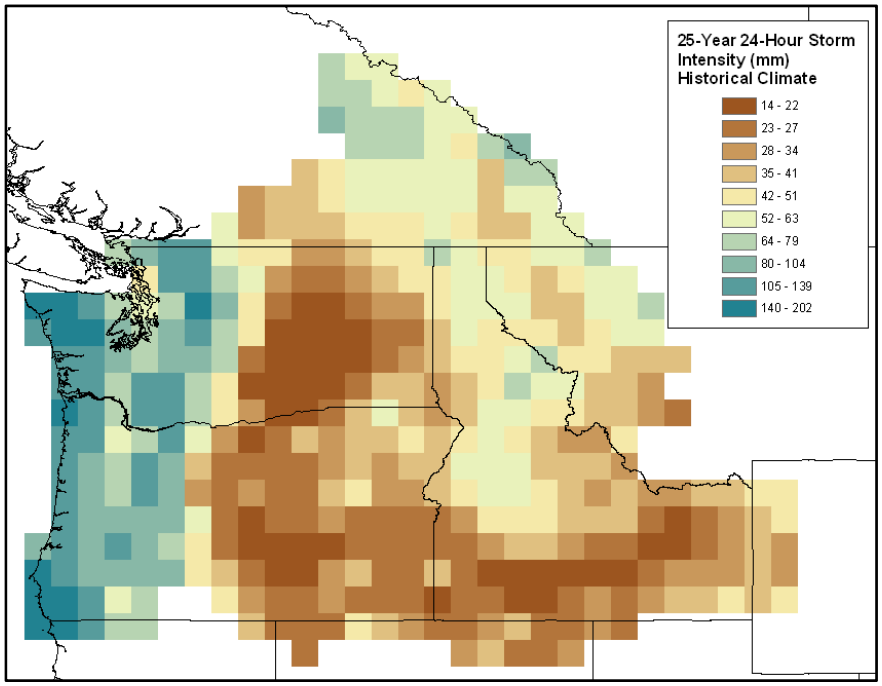

Appendix Figure 2: Historical 25-Year 24-Hour Storm Intensity (mm) as fit to GEV distribution using the method of L-moments

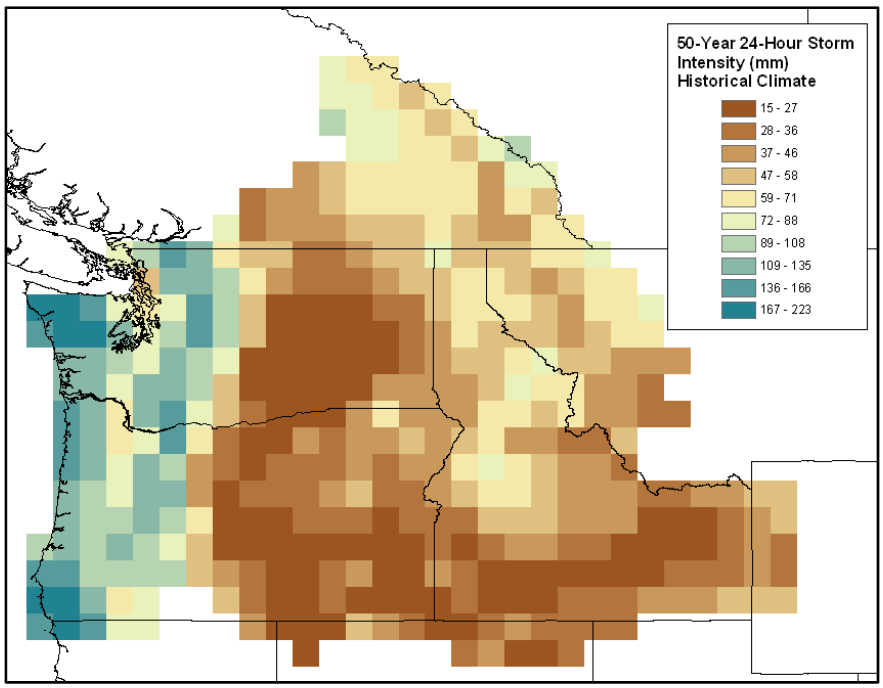

Appendix Figure 3: Historical 50-Year 24-Hour Storm Intensity (mm) as fit to GEV distribution using the method of L-moments

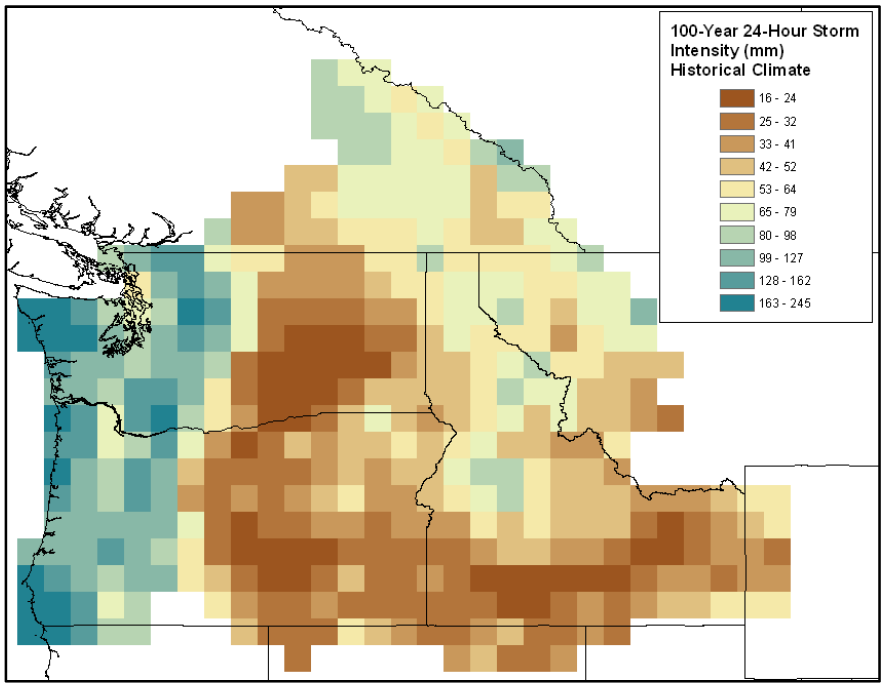

Appendix Figure 4: Historical 100-Year 24-Hour Storm Intensity (mm) as fit to GEV distribution using the method of L-moments

A.2 Monte Carlo Simulated Runoff Depths for Future Storm Events

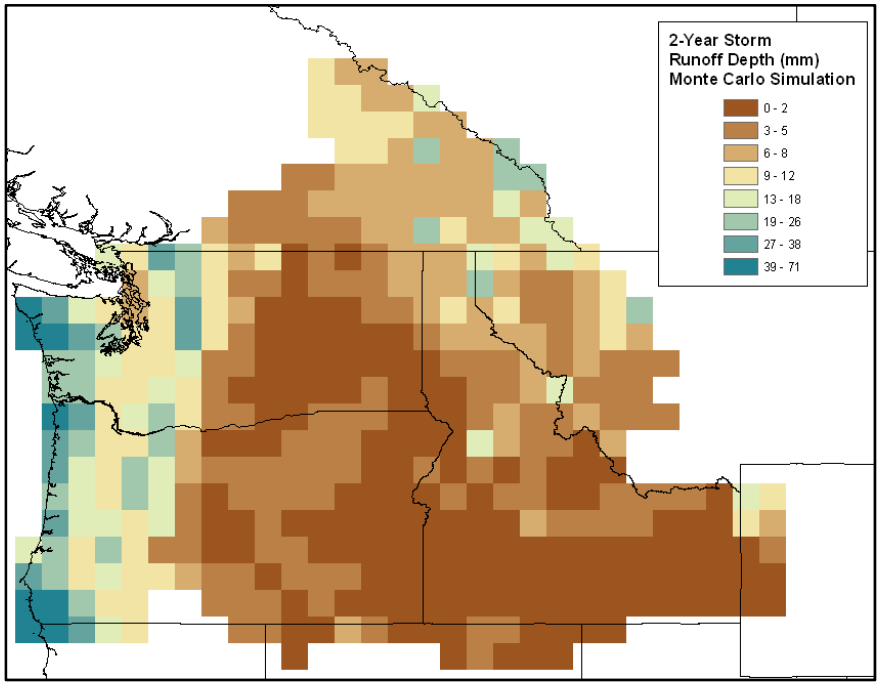

Appendix Figure 5: Runoff depth due to the 2-year storm with 5000 realizations of random selection for emissions scenario, GCM, soil moisture and snow water-equivalent

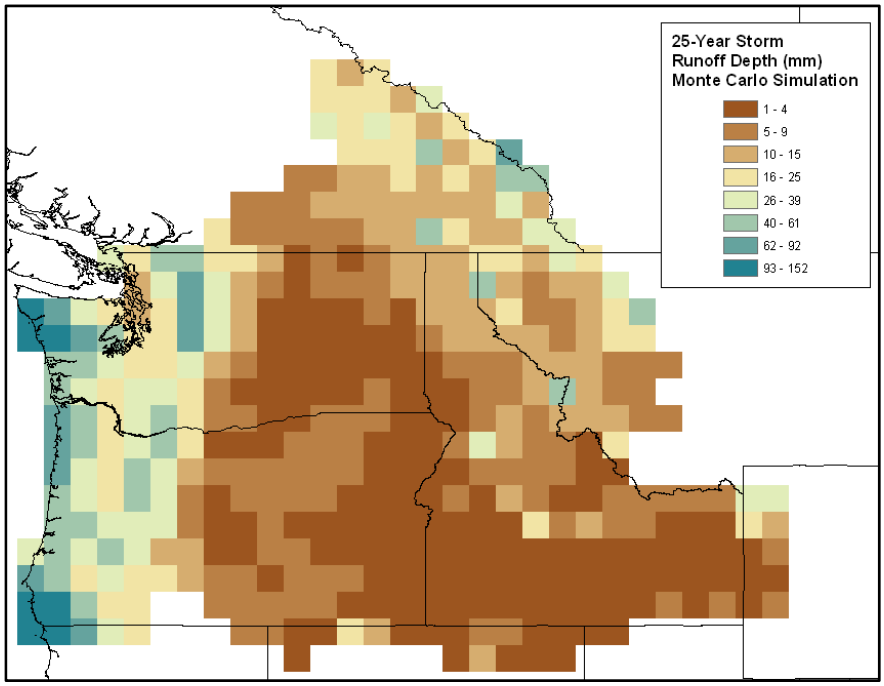

Appendix Figure 6: Runoff depth due to the 25-year storm with 5000 realizations of random selection for emissions scenario, GCM, soil moisture and snow water-equivalent

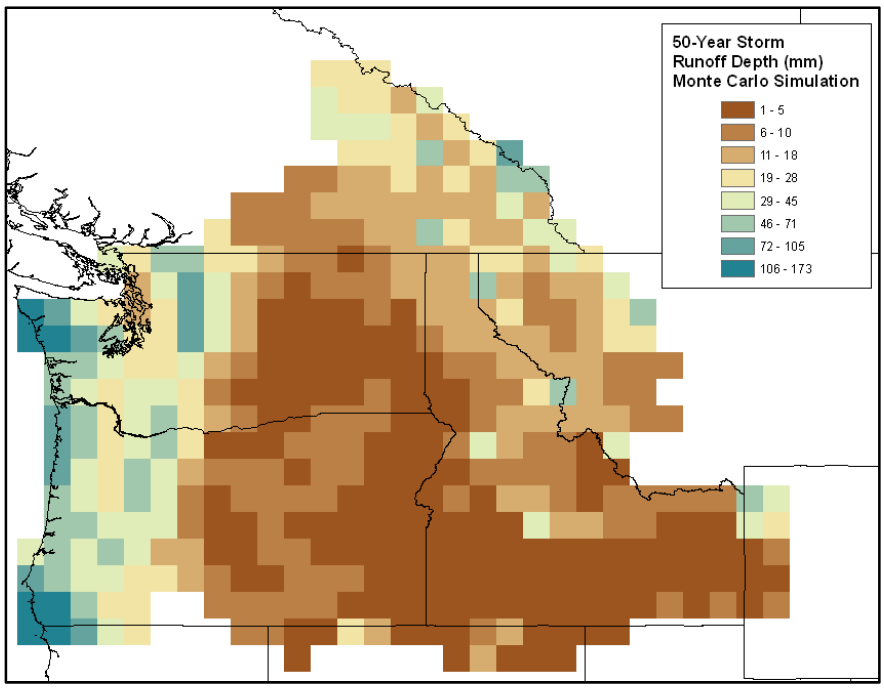

Appendix Figure 7: Runoff depth due to the 50-year storm with 5000 realizations of random selection for emissions scenario, GCM, soil moisture and snow water-equivalent

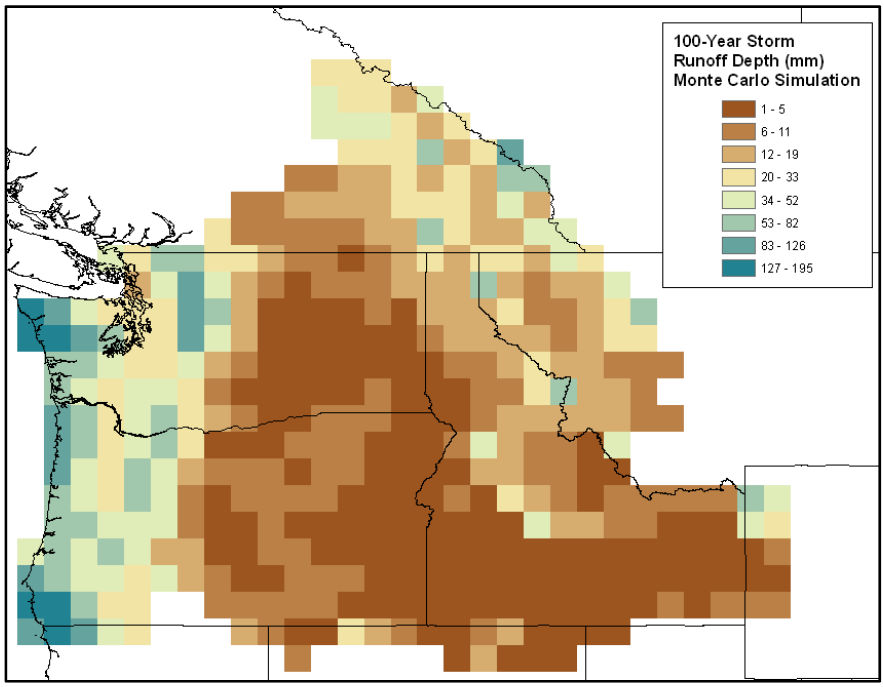

Appendix Figure 8: Runoff depth due to the 100-year storm with 5000 realizations of random selection for emissions scenario, GCM, soil moisture and snow water-equivalent

A.3 GEV Model and L-Moment Summary Statistics for Historical Rainfall Data

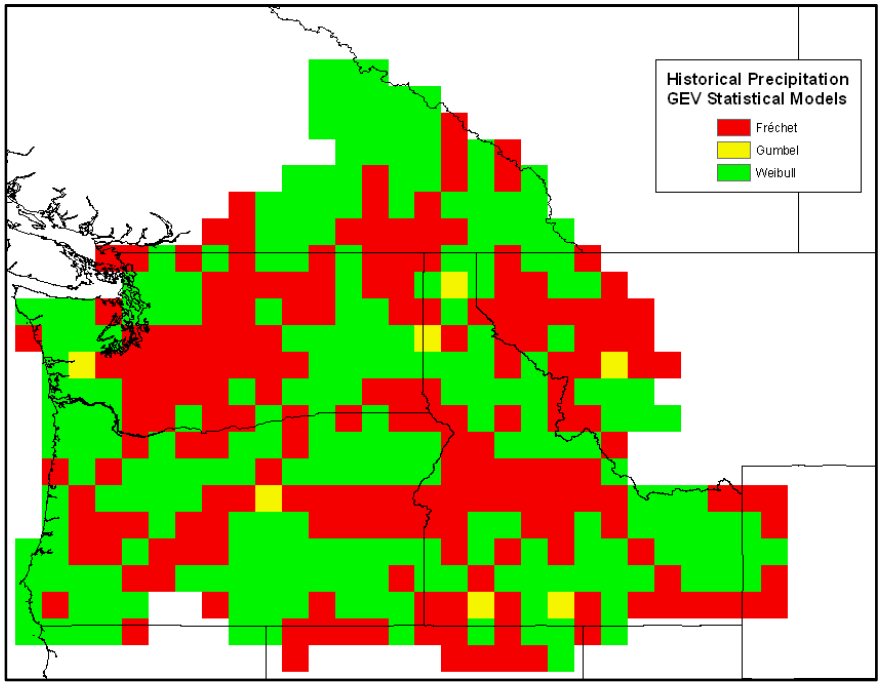

Appendix Figure 9: Generalized Extreme Value distribution type as determined by the κ parameter, with negative values yielding the Fréchet distribution, positive values the Weibull distribution, and values around zero the Gumbel distribution

The GEV model is determined by the kappa parameter (as in 2.4.1). The kappa parameter is derived from the sample L-moments. The Gumbel distribution ($\kappa=0$) was given here with a tolerance of 0 ± 0.0015. This study used the method in Hosking and Wallis (1997) for fitting the GEV distribution to sample L-moments. Pooled regional estimates (as in Hosking and Wallis 1997) were not used due to the application of gridded data which are already interpolated from gauge data (Hamlet and Lettenmaier 2005).

The following figures demonstrate the measures of dispersion and shape derived from the sample moments, and exist on a range of [0,1] (Hosking and Wallis 1997). They are analogous

to conventional moment measures (Hosking and Wallis 1997). Regions with similar values for L-CV, L-skewness and L-kurtosis typically have similar rainfall regimes (Hosking and Wallis 1997). However, due to the large area of each grid cell the apparent homogeneity of the grid cells is lost.

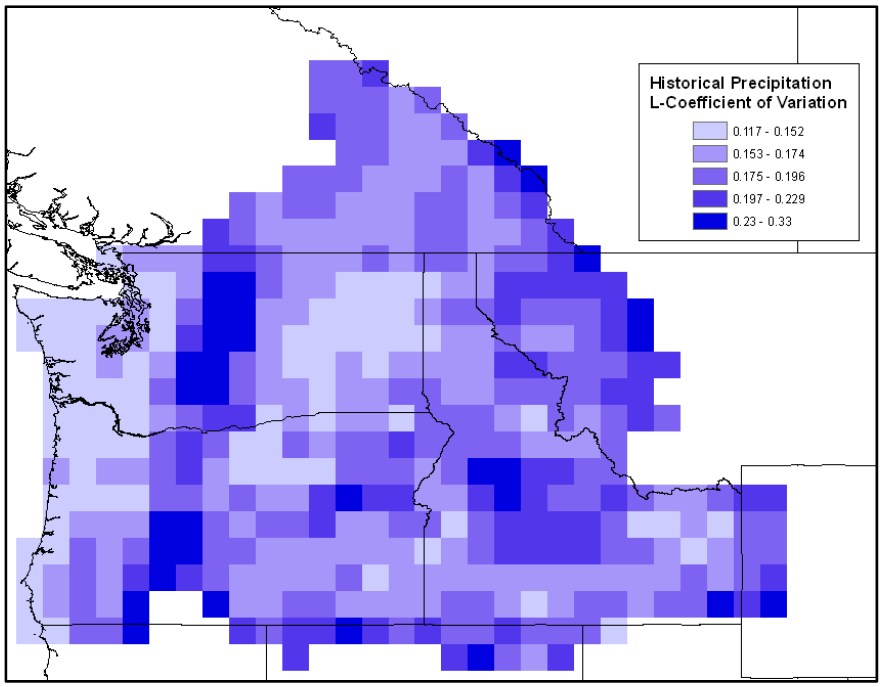

Appendix Figure 10: L-coefficient of variation for historical annual maximum precipitation values

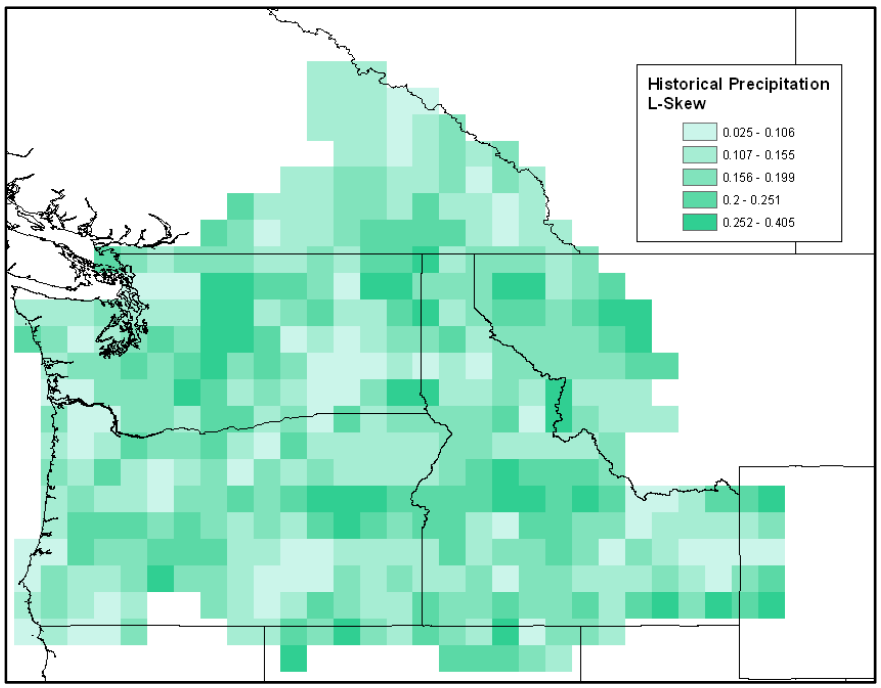

Appendix Figure 11: L-skewness values for historical annual maximum precipitation

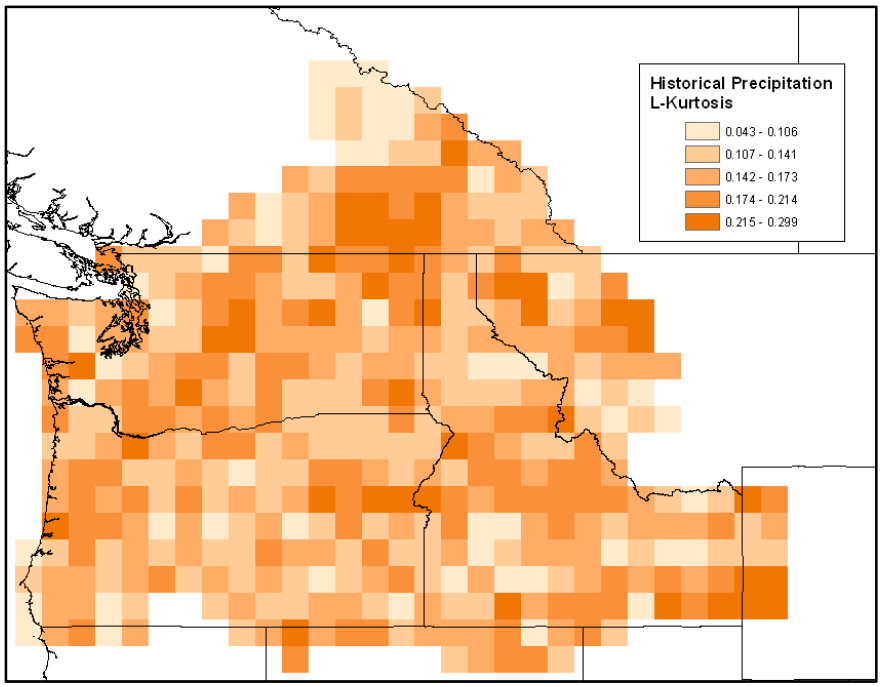

Appendix Figure 12: L-kurtosis values for historical annual maximum precipitation